Meteorological Model Performance
2007 Fine Scale Platform

1. INTRODUCTION

The Weather Research and Forecasting model (WRF) has been applied for the entire year of 2007 to support emissions and photochemical modeling applications. These meteorological fields are intended for use in emissions and photochemical modeling scenarios at a relatively fine scale in order to support assessments of ozone and PM2.5.

The WRF model was applied to a four 4-km domains across the US. These domains included all of California, the metropolitan area of Detroit, metropolitan area of Atlanta and the Northeast corridor. Model simulations were initialized directly from meteorological analysis data. Model parameterizations and options outlined in this document were chosen based on a series of sensitivity runs performed by U.S. Environmental Protection Agency (USEPA) Office of Research and Development that provided an optimal configuration based on temperature, mixing ratio, and wind field. All WRF simulations were done by Computer Sciences Corporation (CSC) under contract to the USEPA.

2. MODEL CONFIGURATION

2.1 Configuration of the Detroit (4DET), Atlanta (4ATL) and Northeast (4NE) Domains

Meteorological inputs are generated with version 3.3 of the WRF model, Advanced Research WRF (ARW) core (Skamarock, 2008). Selected physics options include Pleim-Xiu land surface model (Pleim and Xiu, 2003), Asymmetric Convective Model version 2 planetary boundary layer scheme (Pleim, 2007), Kain-Fritsch cumulus parameterization (Kain, 2004) utilizing the moisture-advection trigger (Ma and Tan, 2009), Morrison double moment microphysics (Morrison et al., 2009), and RRTMG longwave and shortwave radiation schemes (Iacono et al., 2008).

The WRF model was initialized using the 12NAM analysis product provided by NCDC. Where 12NAM data was unavailable, the 36 km AWIP/EDAS analysis (ds609.2) from NCAR was used. Analysis nudging for temperature, wind, and moisture is applied above the boundary layer only. The model simulations were conducted in 5.5 day blocks with soil moisture and temperature carried from one block to the next via the ipxwrf program (Gilliam and Pleim, 2010). Landuse and land cover data are based on the U.S. Geological Survey (USGS) data.

Figures 2.1 through 2.3 show the 4DET, 4ATL and 4NE domains. These domains utilize Lambert conformal projections with true latitudes of 33 and 45 degrees north. All cells are 4 km^2. The atmosphere is resolved with 35 vertical layers up to 50 mb, with the thinnest layers being nearest the surface to better resolve the planetary boundary layer (PBL).

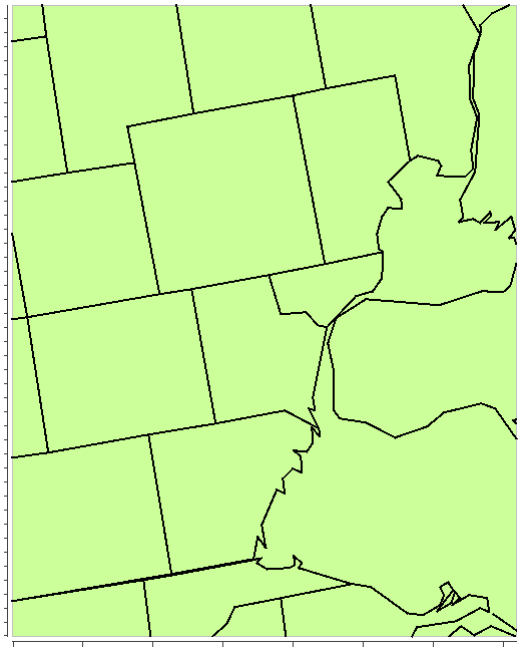

Figure 2.1 Map of WRF model domain: 4DET

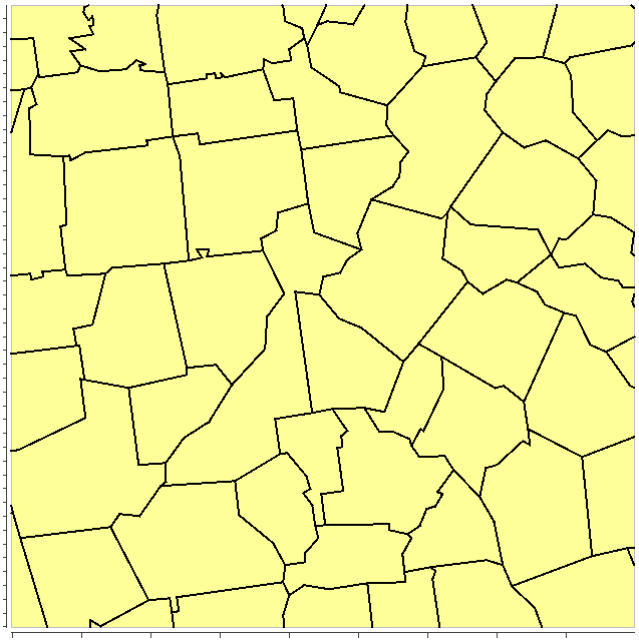

Figure 2.2 Map of WRF model domain: 4ATL

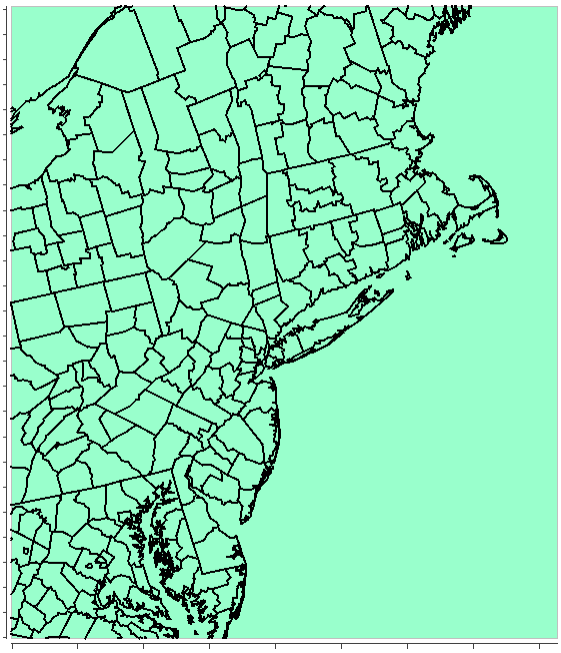

Figure 2.3 Map of WRF model domain: 4NE

2.2 Configuration of the California (4CALNEX) Domain

Meteorological inputs are generated with version 3.3 of the WRF model, ARW core. Selected physics options include Noah land surface model (Ek et al., 2003), Mellor-Yamada-Janjic planetary boundary layer scheme (Janjic, 1994), Kain-Fritsch cumulus parameterization (Kain, 2004) utilizing the moisture-advection trigger (Ma and Tan, 2009), Thompson microphysics (Thompson et al., 2008), and RRTM longwave (Mlawer et al., 1997) and Goddard shortwave (Chou and Suarez, 1994) radiation schemes (Fast et al., 2012).

The WRF model was initialized using the 12NAM analysis product provided by NCDC. Where 12NAM data was unavailable, the 36 km AWIP/EDAS analysis (ds609.2) from NCAR was used. Analysis nudging for temperature, wind, and moisture is applied above the boundary layer only. The model simulations were conducted in 5.5 day blocks with soil moisture and temperature carried from one block to the next via the **ipxwrf** program (Gilliam and Pleim, 2010). Landuse and land cover data are based on the U.S. Geological Survey (USGS) data.

Figure 2.4 shows the 4CALNEX domain, which utilizes a Lambert conformal projection with true latitudes of 33 and 45 degrees north. All cells are 4 km^2. The atmosphere is resolved with 35 vertical layers up to 50 mb, with the thinnest layers being nearest the surface to better resolve the PBL.

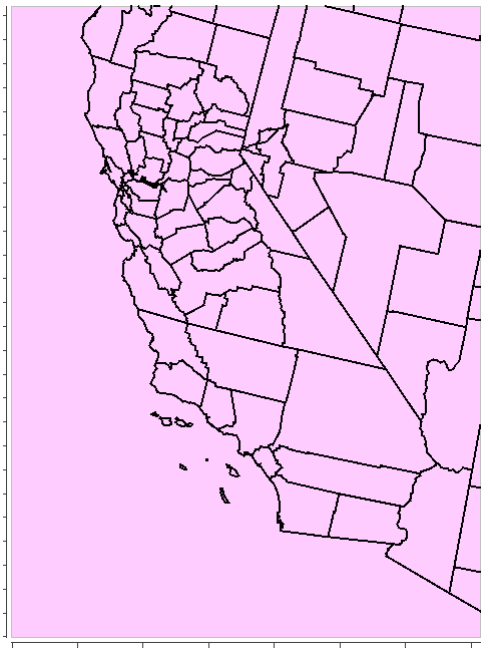

Figure 2.4 Map of WRF model domain: 4CALNEX

2.3 WRF Conversion to Photochemical Model Inputs

CMAQ-ready meteorological input files were prepared using the Meteorology-Chemistry Interface Processor (MCIP) package (Otte and Pleim, 2010). The code is available at www.cmascenter.org. MCIP v4.1.2 was used to generate CMAQ ready meteorological files for all domains.

3 MODEL PERFORMANCE DESCRIPTION

The model simulations are evaluated to determine whether the output fields represent a reasonable approximation of the actual meteorology that occurred during the modeling period. Identifying and quantifying these output fields allows for a downstream assessment of how the air quality modeling results are impacted by the meteorological data.

Performance results are presented to allow those using this data to determine the adequacy of the model simulation for their particular needs.

The observation database for temperature, wind speed and direction, and mixing ratio is based on measurements made at United States and Canadian airports. The observational dataset (ds472) is available from NCAR. Monitors used for evaluation are shown in Figure 3.1.

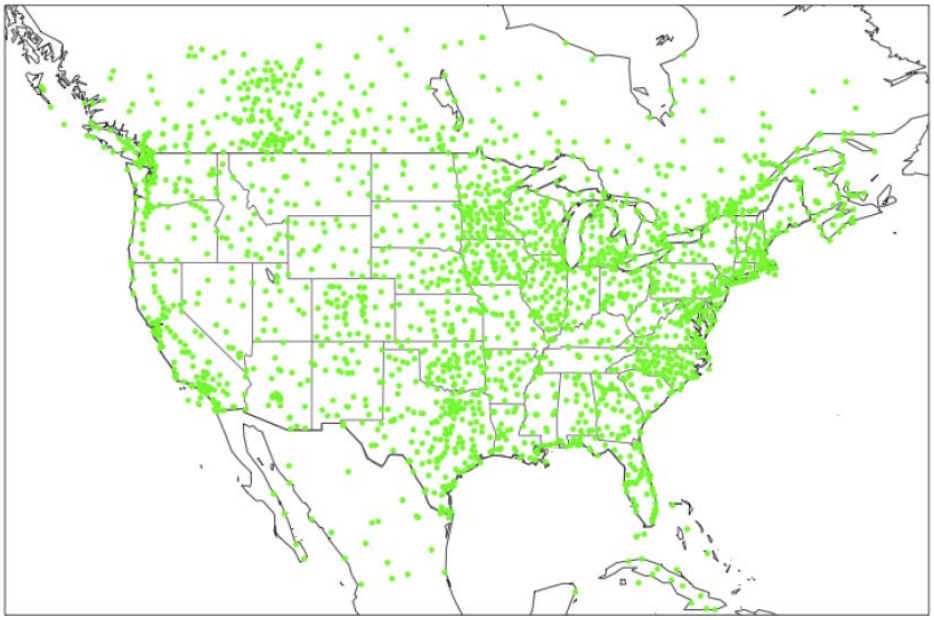

Figure 3.1 Stations used for model performance: ds472 network.

Shortwave downward radiation measurements are taken at SURFRAD (http://www.srrb.noaa.gov/surfrad) and ISIS (http://www.srrb.noaa.gov/isis/index.html) monitor locations. The SURFRAD network consists of 7 sites and the ISIS network consists of 9 sites across the United States (Figure 3.2). A comparison of modeled and observed radiation values was thus only available in the 4NE and 4CALNEX domains as no SURFRAD or ISIS stations were located in the other domains.

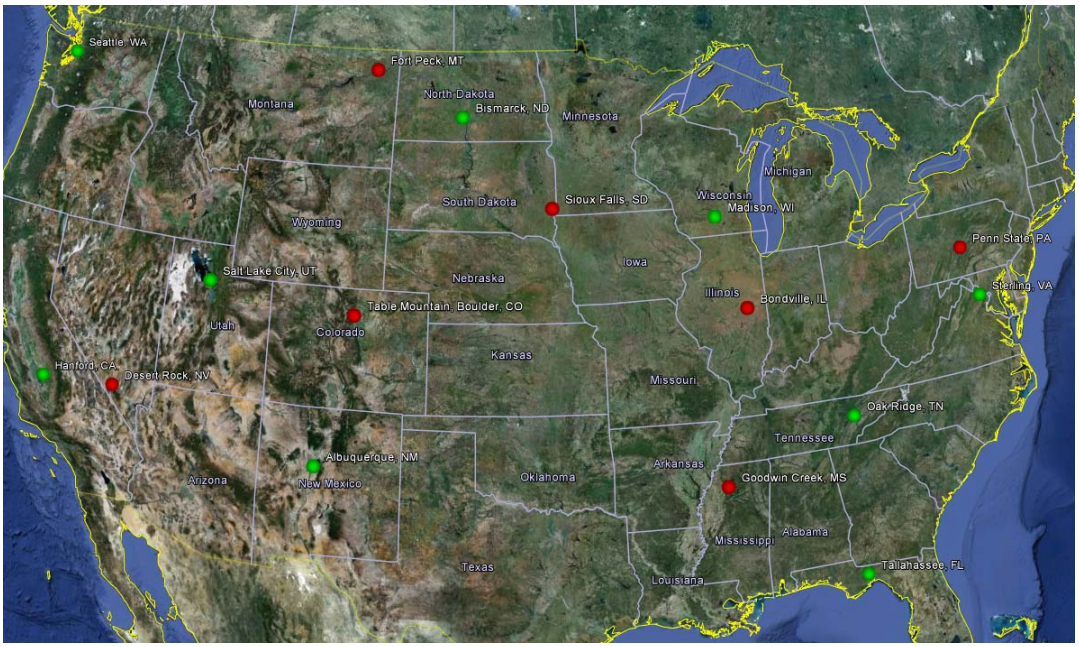

SURFRAD

ISIS

Figure 3.2. Location of ISIS and SURFRAD radiation monitors.

Rainfall analysis estimated by the Parameter-elevation Regressions on Independent Slopes Model (PRISM) is approximately 2 to 4 km resolution and is compared to model estimates. The rainfall analysis data does not include any portion of Canada, Mexico, or anywhere off-shore of the United States. The rainfall analysis is re-projected to the modeling domain for direct qualitative comparison to model estimates. Rainfall performance is examined spatially using side-by-side comparisons of monthly total rainfall plots.

Model performance is described using quantitative metrics: mean bias, mean (gross) error, fractional bias, and fractional error (Boylan and Russell, 2006). These metrics are useful because they describe model performance in the measured units of the meteorological variable and as a normalized percentage. Since wind direction is reported in compass degrees, estimating performance metrics is problematic as modeled and observed northerly winds may be similar but differences would result in a very large artificial bias. Wind field displacement, or the difference in the U and V vectors between modeled (M) and observed (O) values, is used to assess wind vector performance (Equation 1). Performance is best when these metrics approach 0.

(1) Wind displacement (km) = $(\mathbf{U}_M - \mathbf{U}_O + \mathbf{V}_M - \mathbf{V}_O)$*(1 km/1000 m)*(3600 s/hr)*(1 hr)

The WRF model outputs predictions approximately 15 meters above the surface while observations are at 10 meters. WRF generates output at near instantaneous values (90 second time step) as opposed to longer averaging times taken at monitor stations. This should be considered when interpreting model performance metrics.

3.1 Detroit (4DET) Performance

3.1.1 Wind Field

Wind speed estimates are compared to surface-based measurements made at the ds472 network described earlier. The results are shown below (Figure 3.1.1). The edges of the box plots represent the 25^{th} and 75^{th} percentiles and edges of the whiskers represent the 10^{th} and 90^{th} percentiles. These plots show the hourly bias (model-observation) by month and by hour of the day. Also included are mean error, fractional bias, and fractional error.

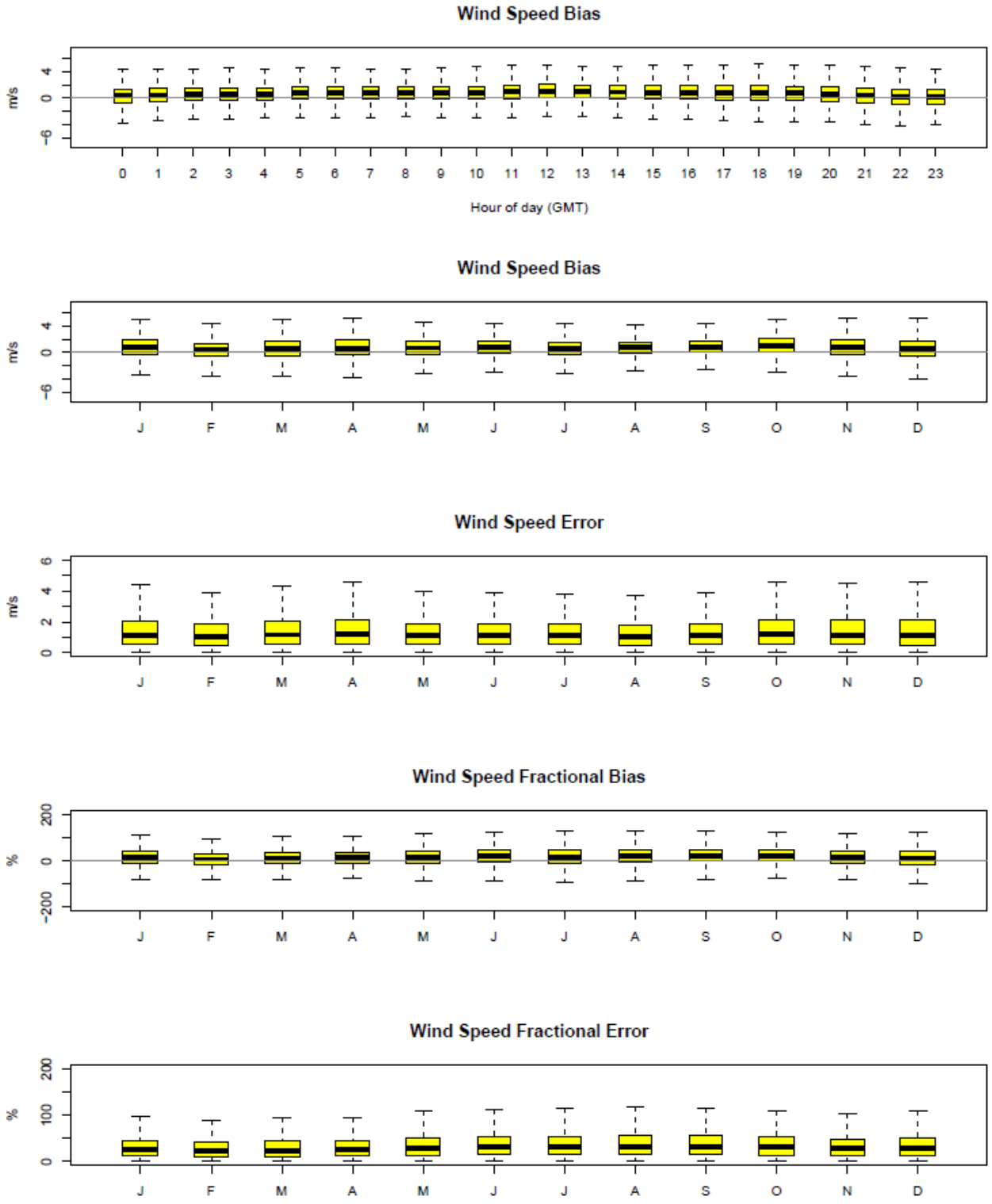

Figure 3.1.1. Distribution of hourly wind speed bias by hour and hourly wind speed bias, error, fractional bias, and fractional error by month for 4DET domain.

Wind vector displacement (km) is presented below utilizing the ds472 observation network described earlier (Figure 3.1.2). These plots show the entire distribution of hourly wind displacement by month and by hour of the day.

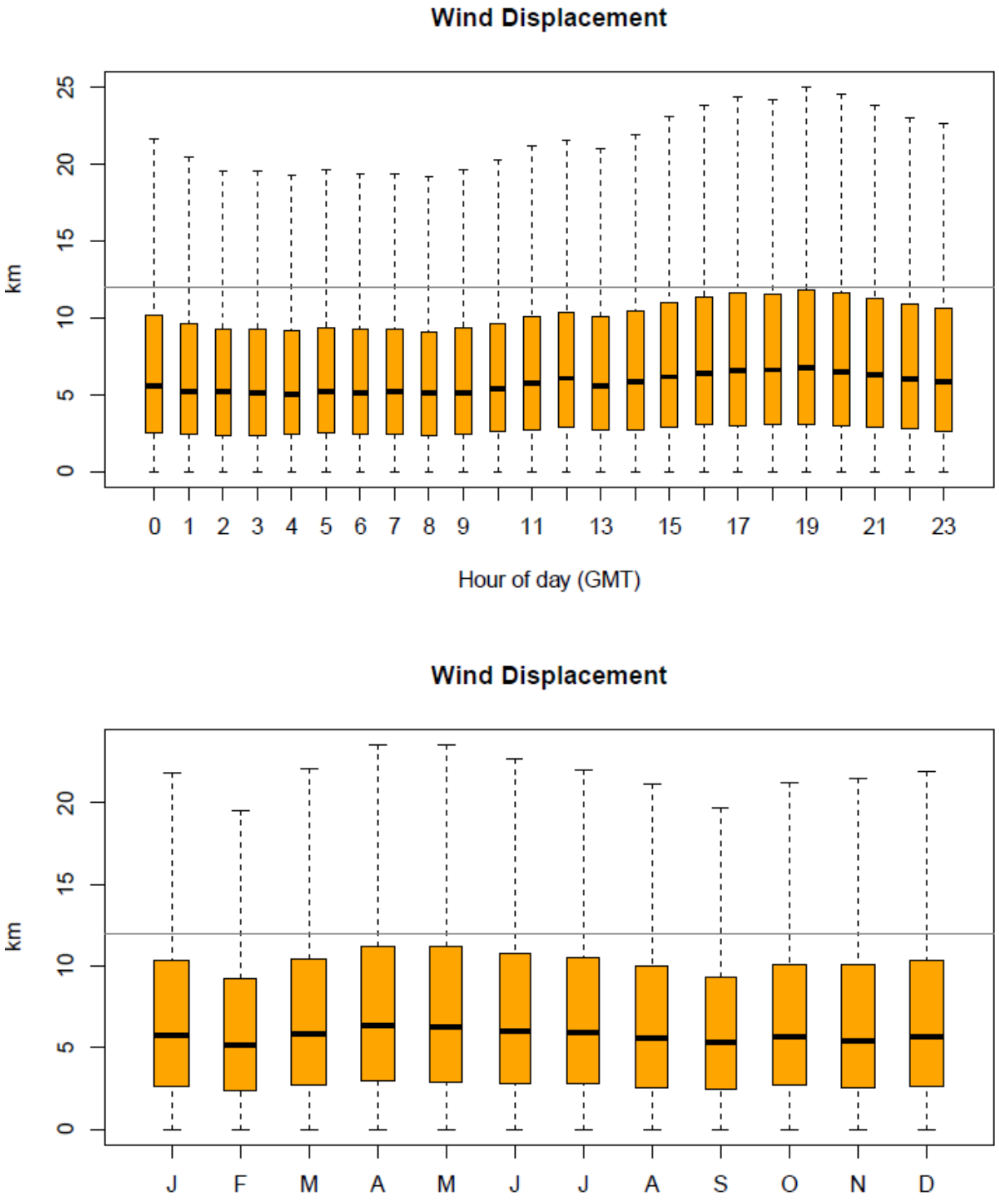

Figure 3.1.2. Distribution of hourly wind displacement by hour and month for the 4DET domain.

3.1.2 Temperature

Temperature estimates are compared to the ds472 observation network described earlier and are presented below for the 4DET domain (Figure 3.1.3).

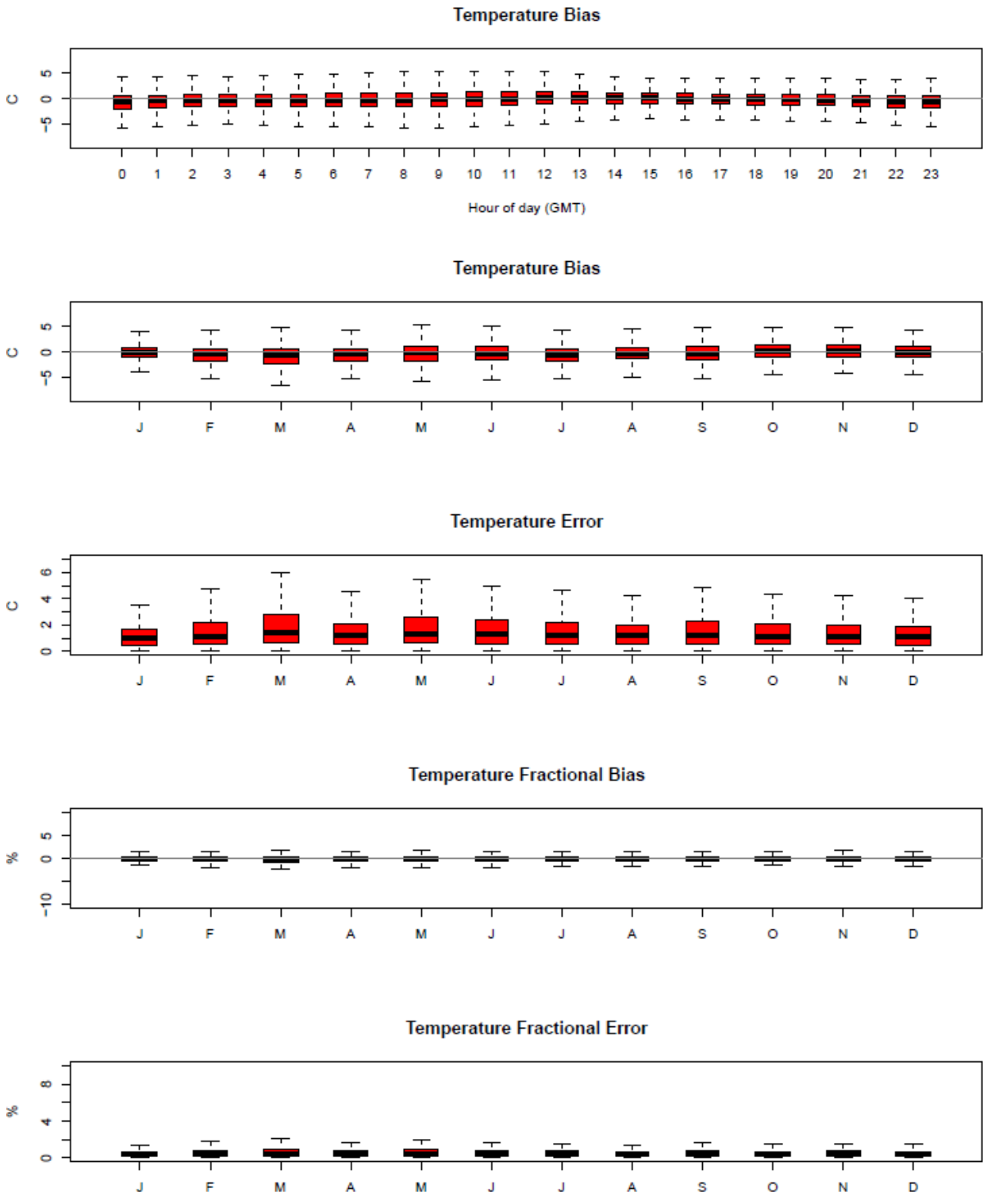

Figure 3.1.3. Distribution of hourly temperature bias by hour and hourly temperature bias, error, fractional bias, and fractional error by month for the 4DET domain.

3.1.3 Mixing Ratio

Water mixing ratio estimates are compared to the ds472 observation network described earlier and are presented below for the 4DET domain (Figure 3.1.4).

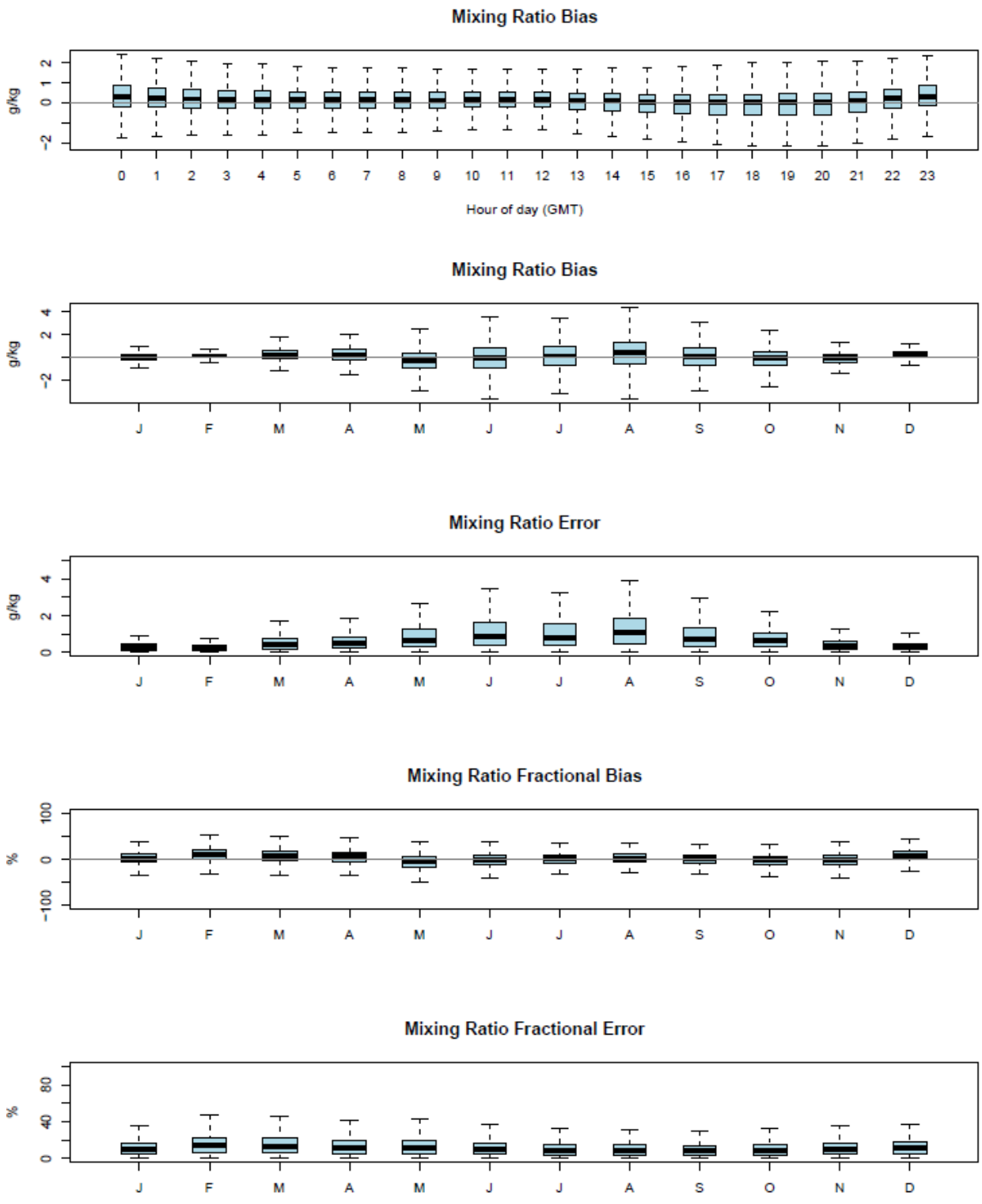

Figure 3.1.4. Distribution of hourly mixing ratio bias by hour and hourly mixing ratio bias, error, fractional bias, and fractional error by month for the 4DET domain.

3.1.4 Precipitation

Monthly total rainfall is plotted for each grid cell to assess how well the model captures the spatial variability and magnitude of convective and non-convective rainfall. As described earlier, the PRISM estimations for rainfall are only within the continental United States. WRF rainfall estimates by month are shown for all grid cells in the domain. Monthly total estimates are shown for the 4DET domain (Figures 3.1.5 through 3.1.8).

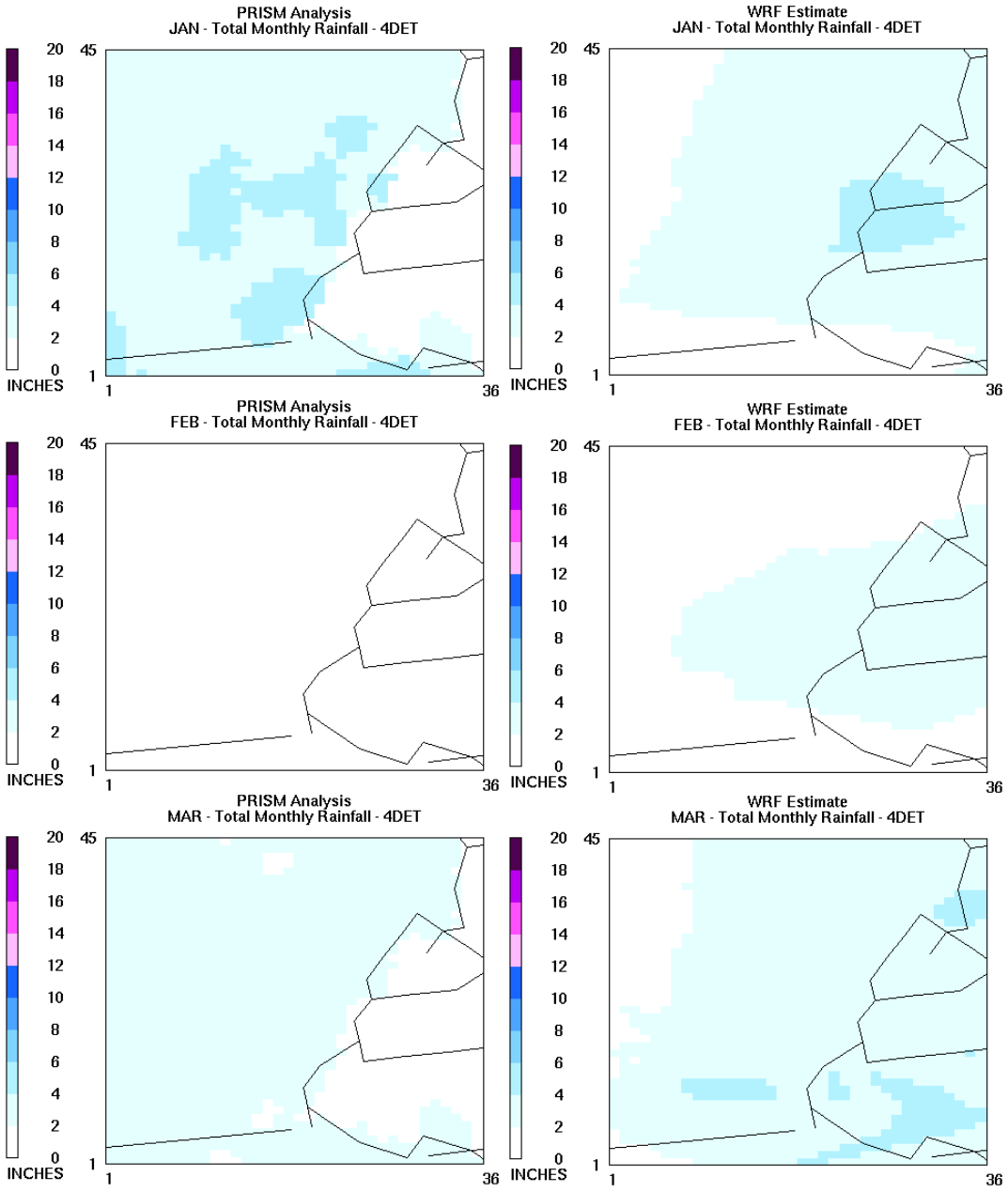

Figure 3.1.5. PRISM analysis (left) and WRF (right) estimated monthly total rainfall for January, February, and March.

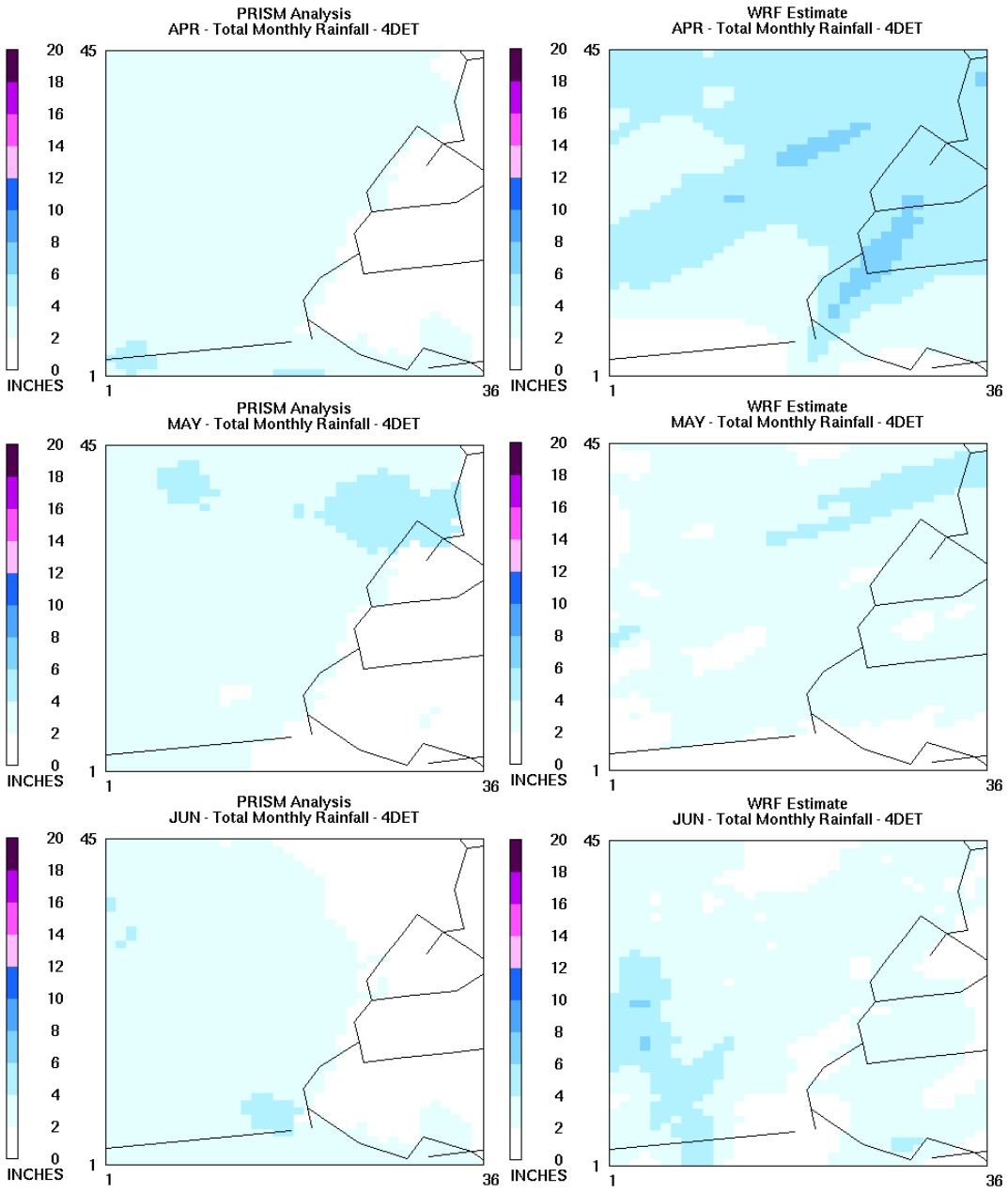

Figure 3.1.6. PRISM analysis (left) and WRF (right) estimated monthly total rainfall for April, May, and June.

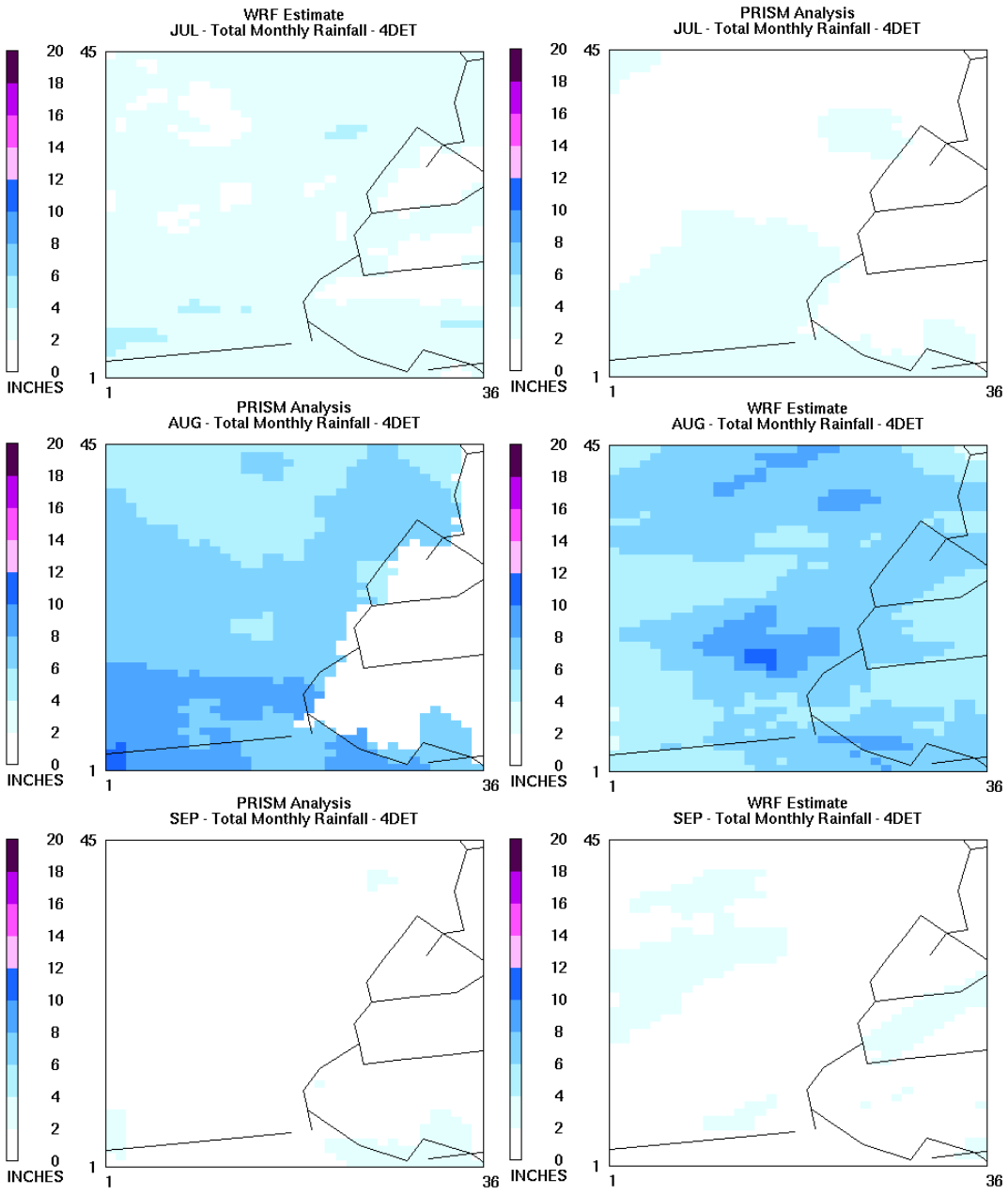

Figure 3.1.7. PRISM analysis (left) and WRF (right) estimated monthly total rainfall for July, August, and September.

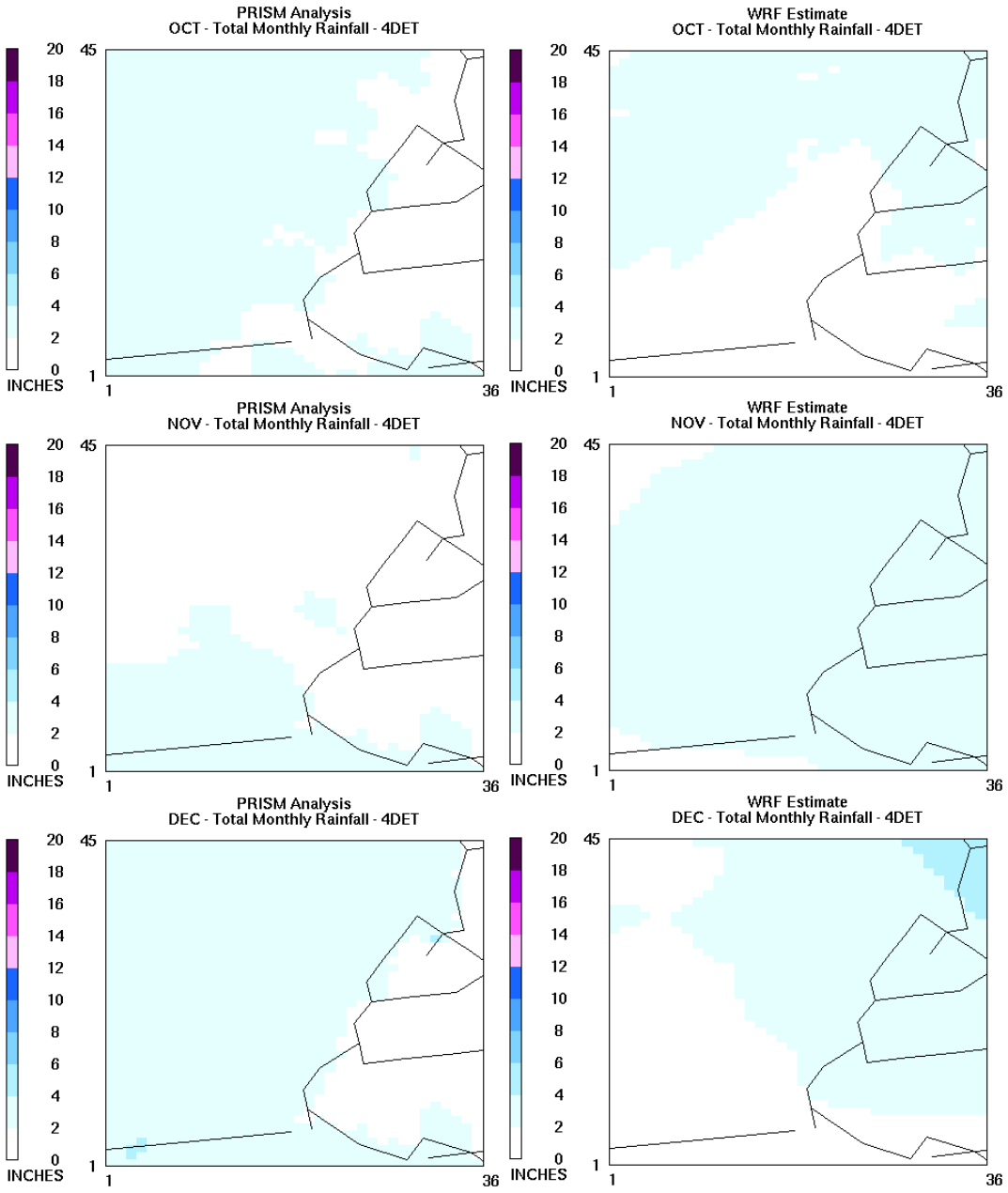

Figure 3.1.8. PRISM analysis (left) and WRF (right) estimated monthly total rainfall for October, November, and December.

3.1.5 Maximum Predicted PBL

Maximum PBL heights are plotted for each grid cell by month for the 4DET domain (Figure 3.1.9). Studies have shown that significantly deep boundary layers may lead to stratospheric intrusion of ozone (Langford and Reid, 1998; Cooper et al., 2005). These plots help assess whether unrealistic intrusion of stratospheric ozone may be occurring.

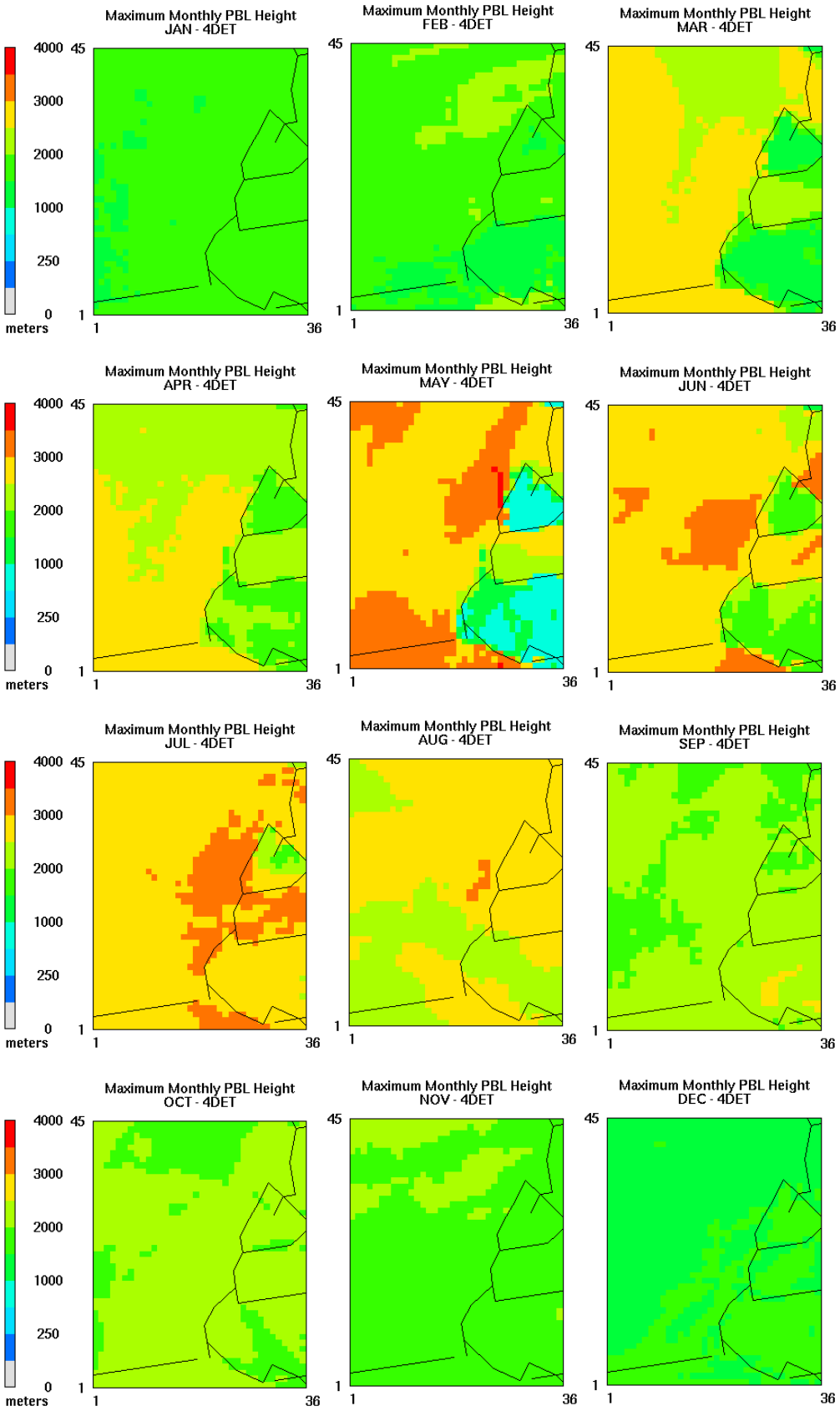

Figure 3.1.9. Monthly maximum PBL heights estimated by WRF for the 4DET domain.

3.2 Atlanta (4ATL) Performance

3.2.1 Wind Field

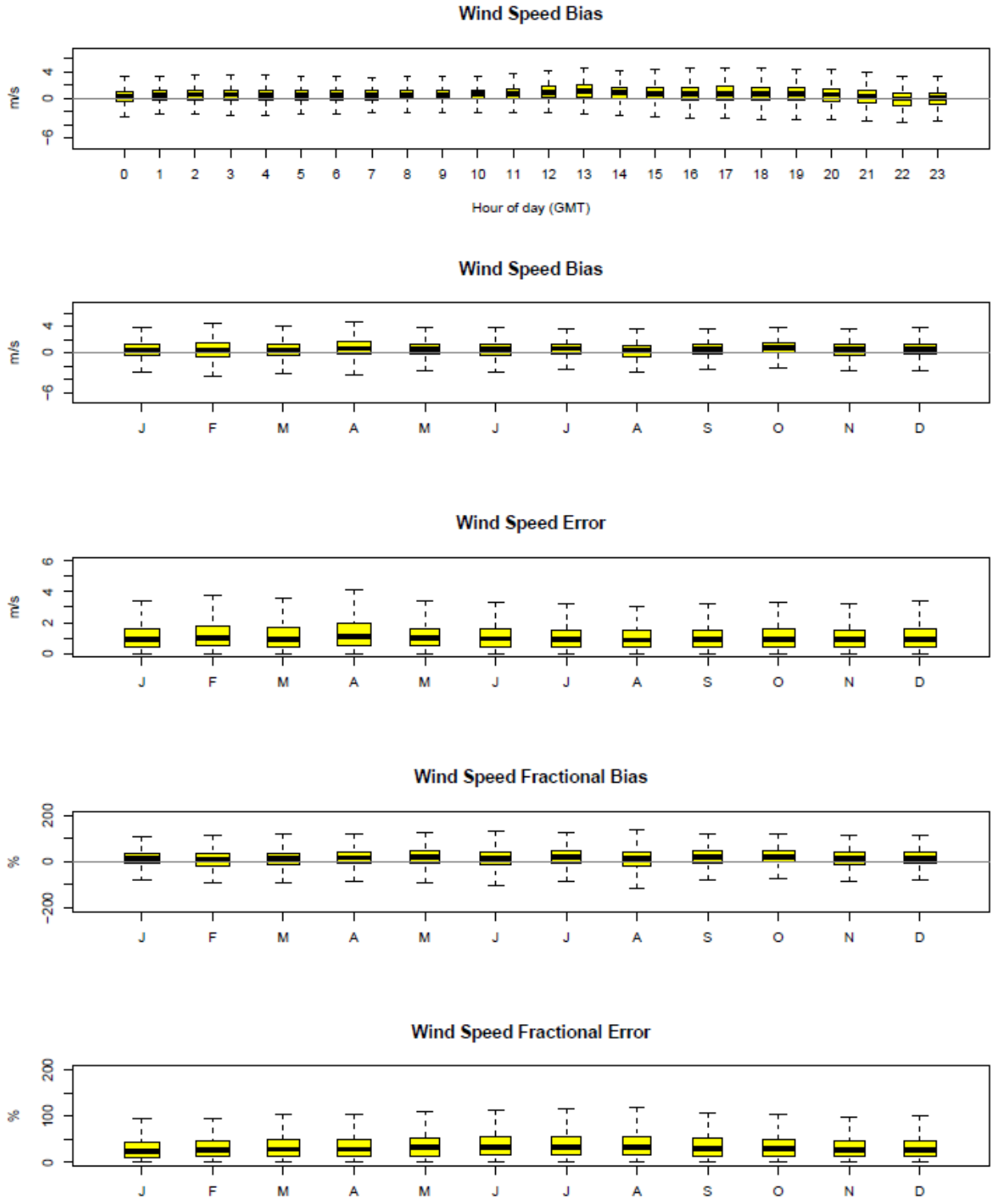

Figure 3.2.1. Distribution of hourly wind speed bias by hour and hourly wind speed bias, error, fractional bias, and fractional error by month for the 4ATL domain.

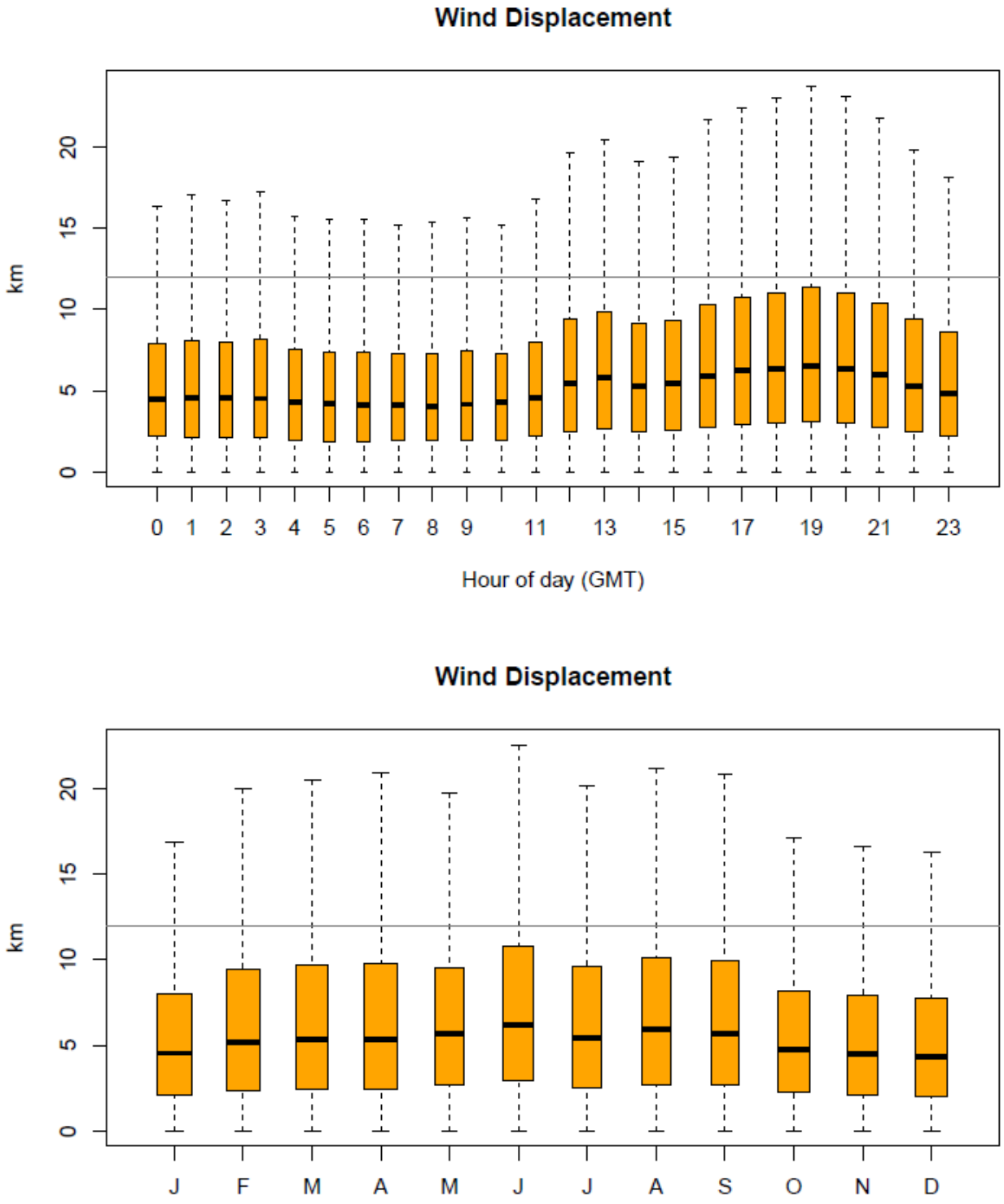

Figure 3.2.2. Distribution of hourly wind displacement by hour and month for the 4DET domain.

3.2.2 Temperature

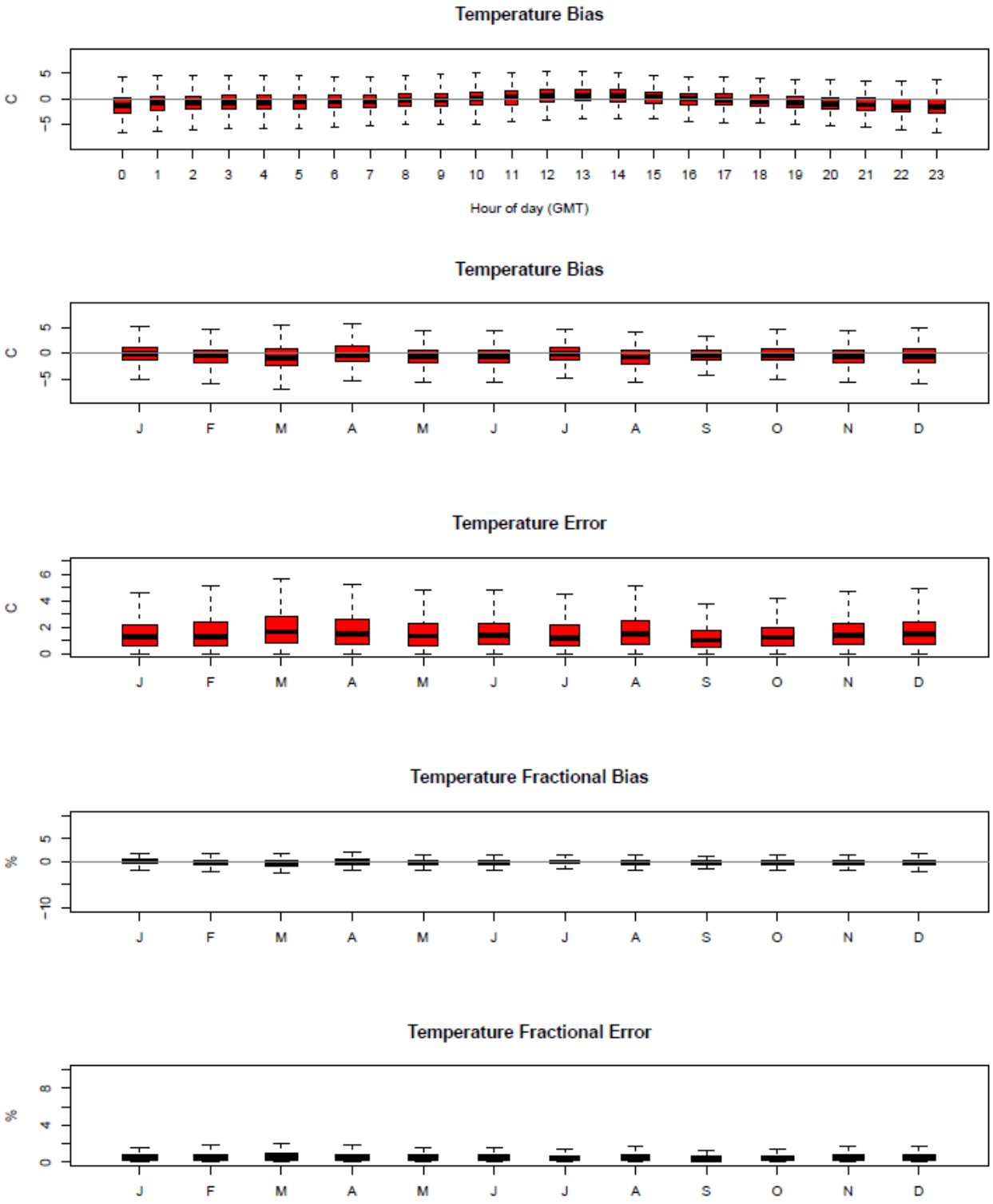

Figure 3.2.3. Distribution of hourly temperature bias by hour and hourly temperature bias, error, fractional bias, and fractional error by month for the 4ATL domain.

3.2.3 Mixing Ratio

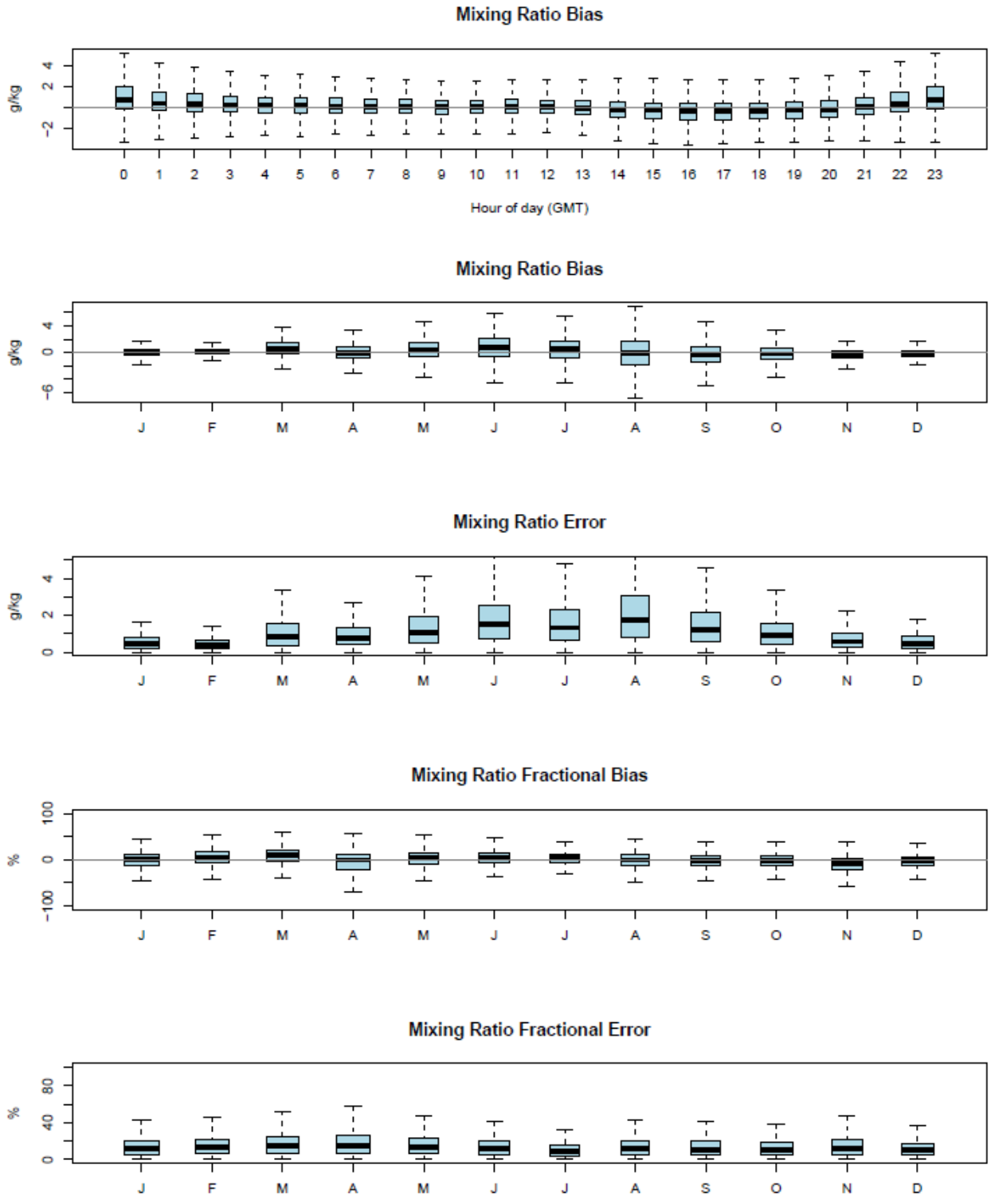

Figure 3.2.4. Distribution of hourly mixing ratio bias by hour and hourly mixing ratio bias, error, fractional bias, and fractional error by month for the 4ATL domain.

3.2.4 Precipitation

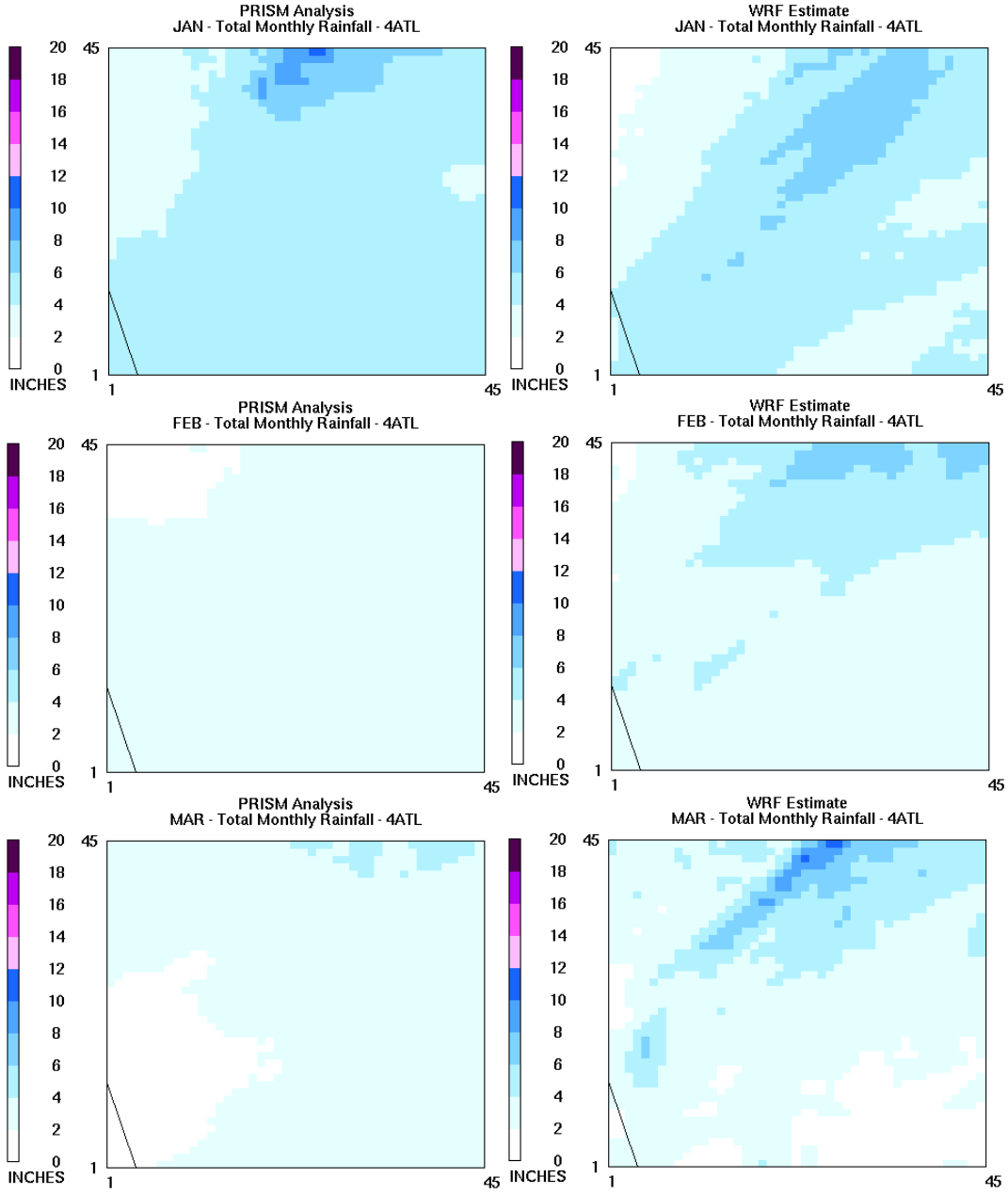

Figure 3.2.5. PRISM analysis (left) and WRF (right) estimated monthly total rainfall for January, February and March for the 4ATL domain.

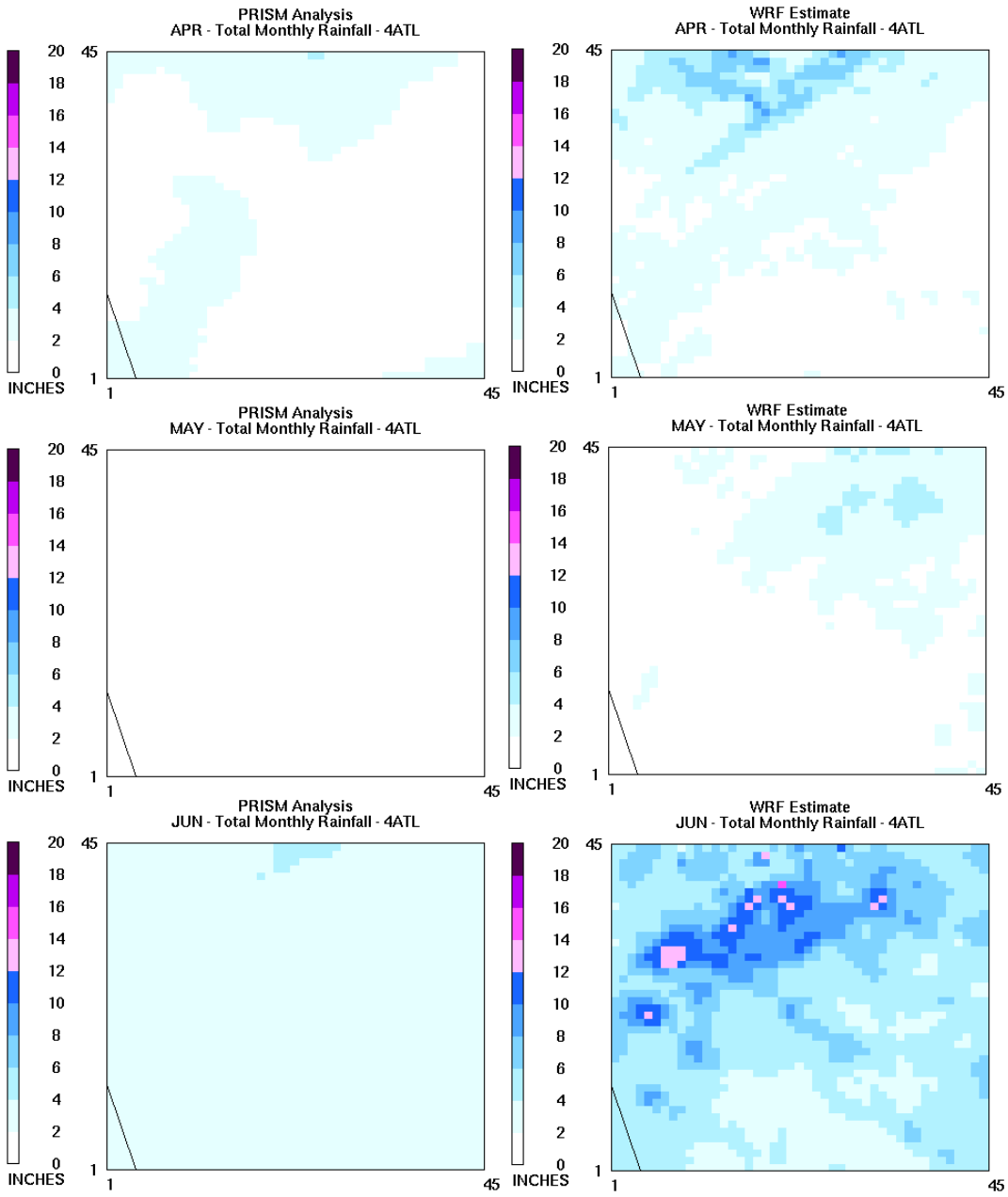

Figure 3.2.6. PRISM analysis (left) and WRF (right) estimated monthly total rainfall for April, May and June for the 4ATL domain.

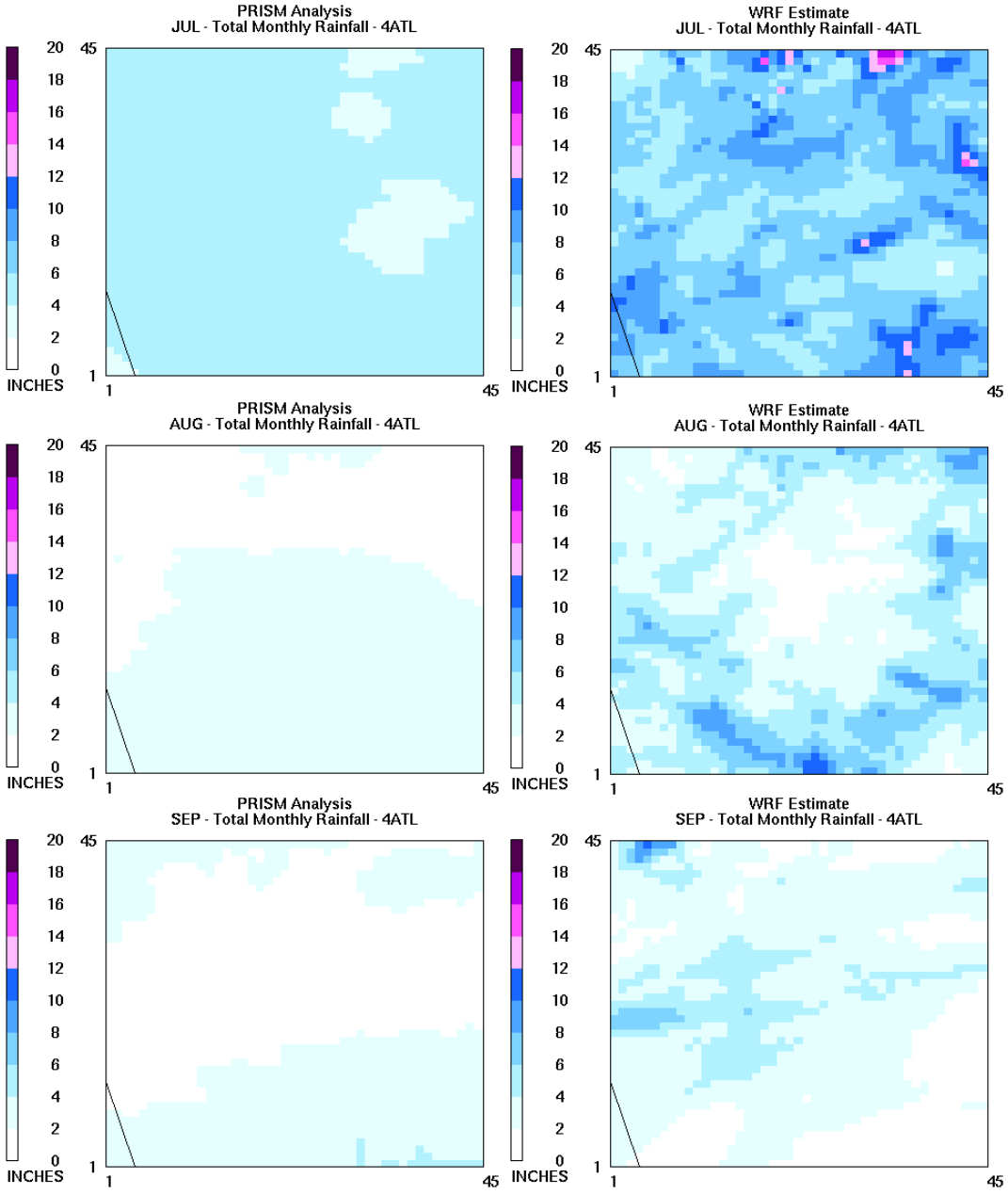

Figure 3.2.7. PRISM analysis (left) and WRF (right) estimated monthly total rainfall for July, August and September for the 4ATL domain.

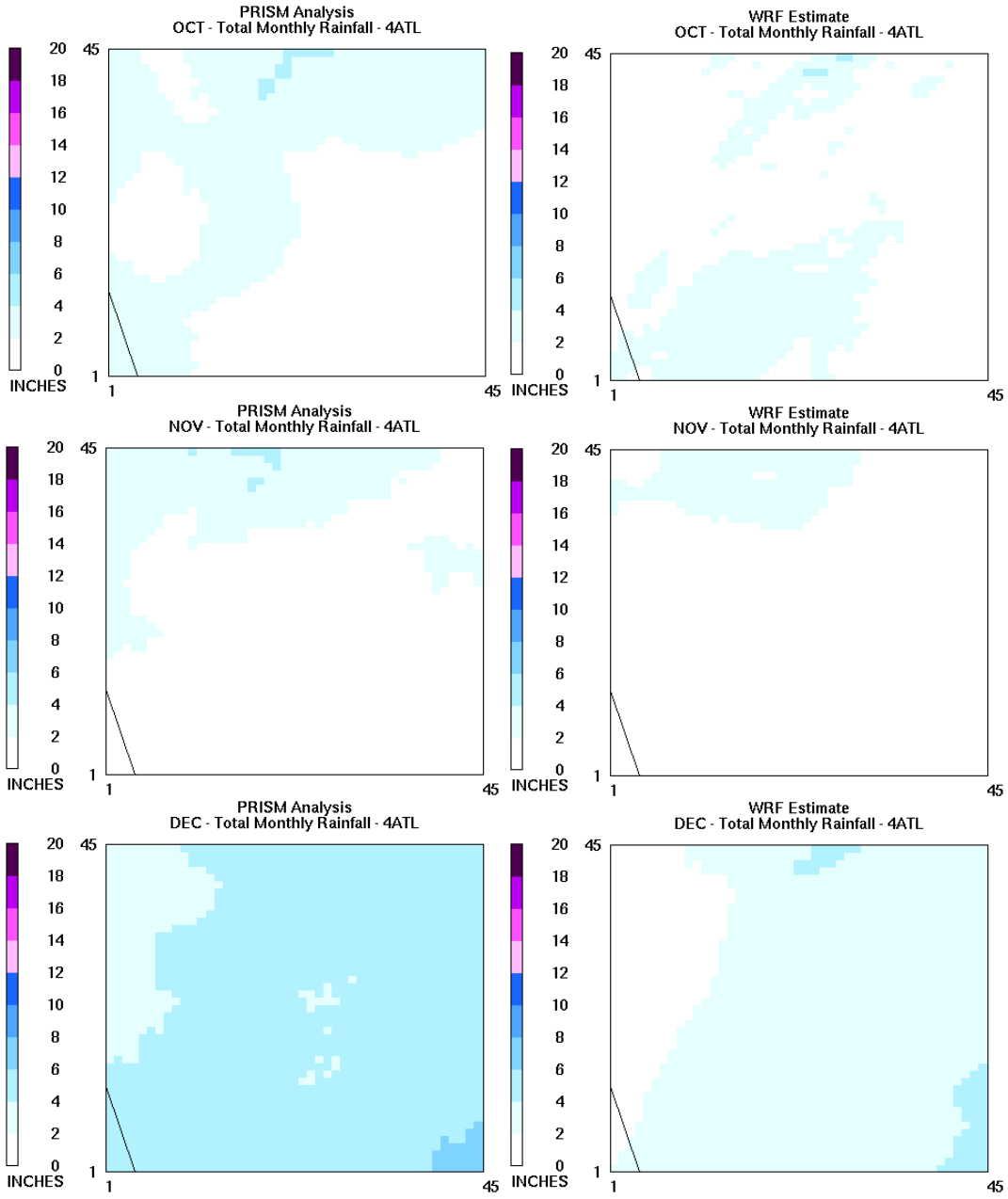

Figure 3.2.8. PRISM analysis (left) and WRF (right) estimated monthly total rainfall for October, November and December for the 4ATL domain.

3.2.5 Maximum Predicted PBL

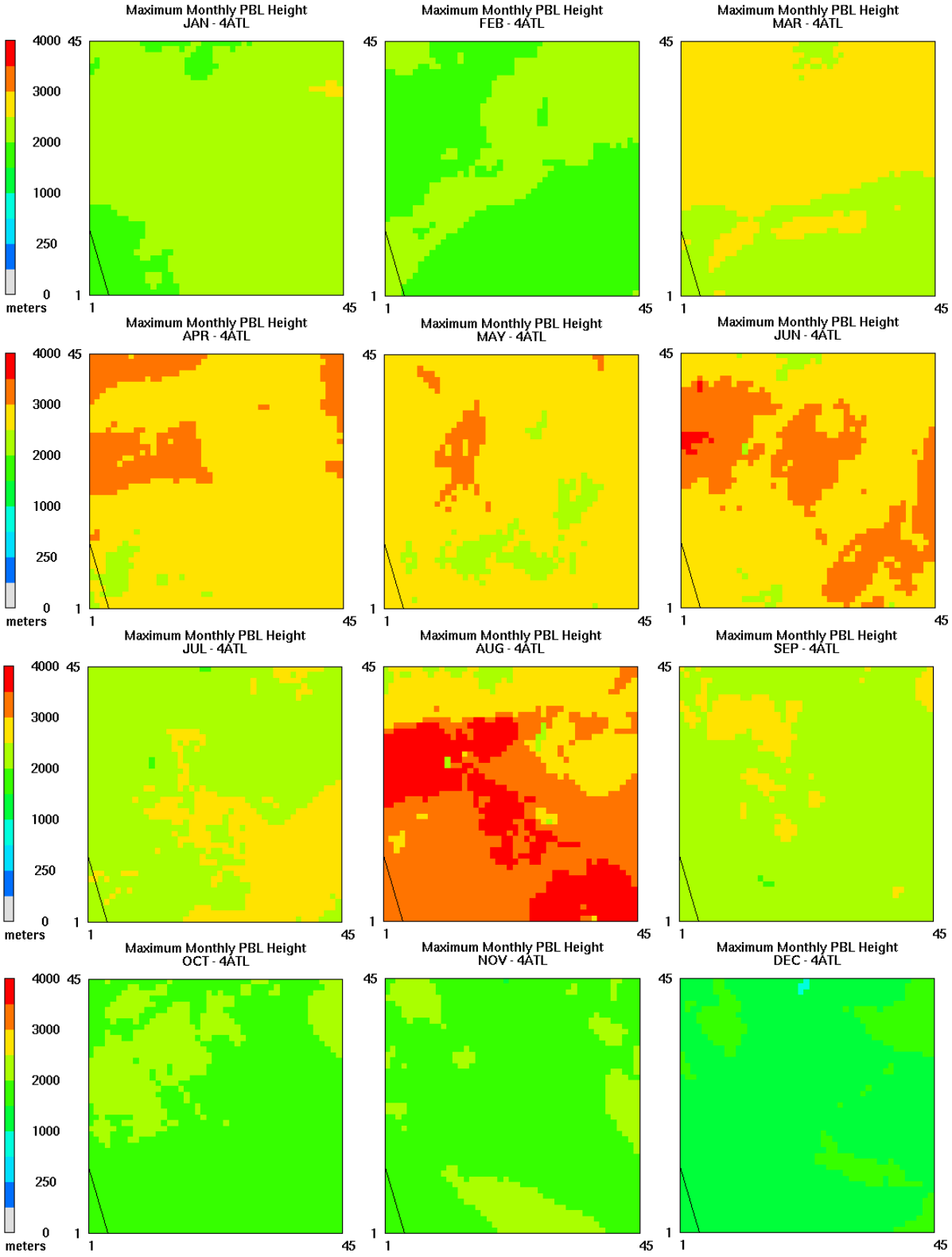

Figure 3.2.9. Monthly maximum PBL heights estimated by WRF for the 4ATL domain.

3.3 Northeast (4NE) Performance

3.3.1 Wind Field

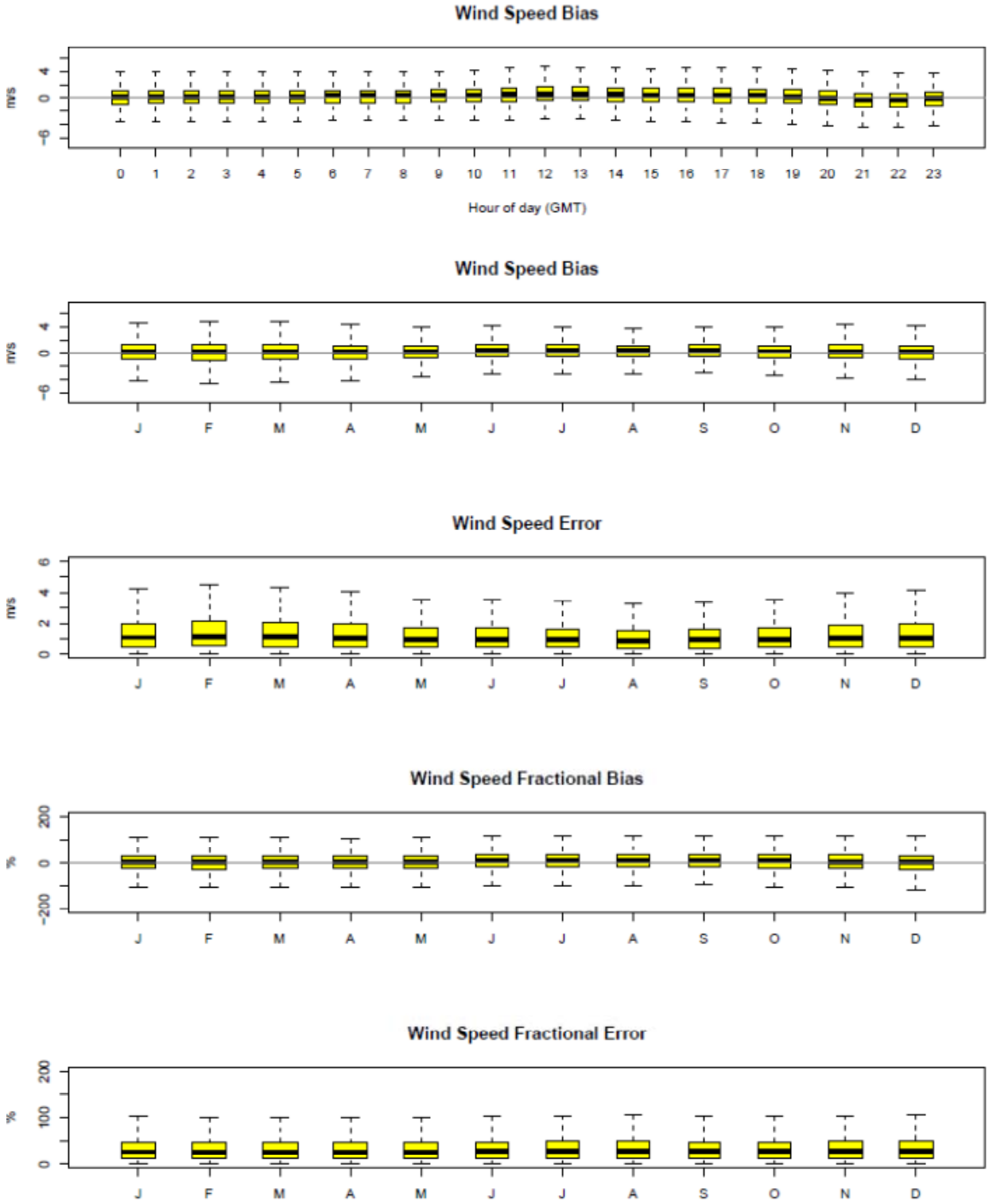

Figure 3.3.1. Distribution of hourly wind speed bias by hour and hourly wind speed bias, error, fractional bias, and fractional error by month for the 4NE domain.

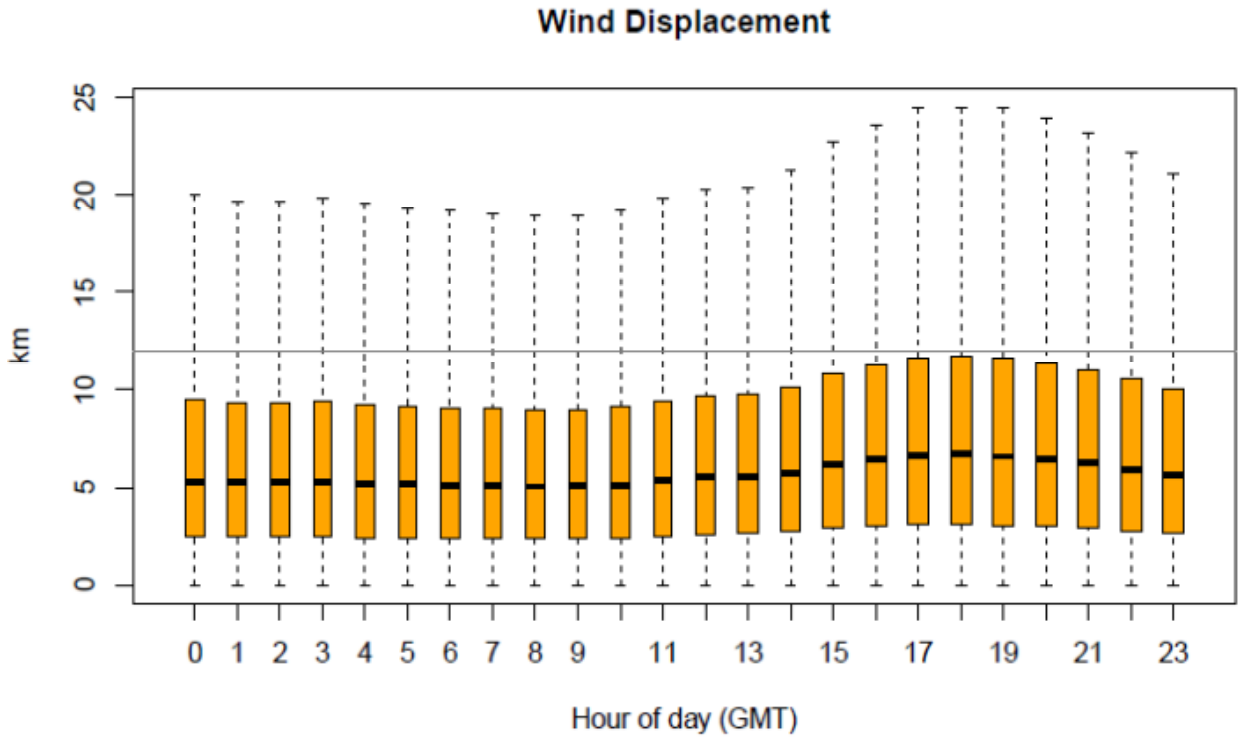

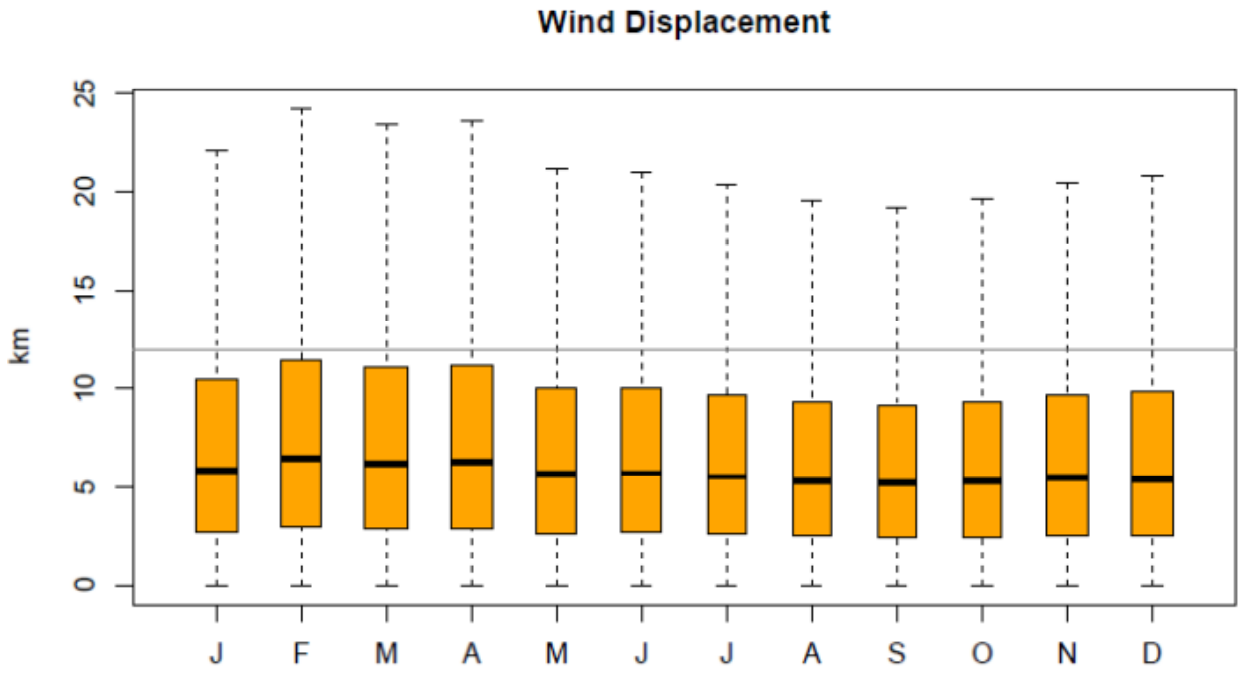

Figure 3.3.2. Distribution of hourly wind displacement by hour and month for the 4NE domain.

3.3.2 Temperature

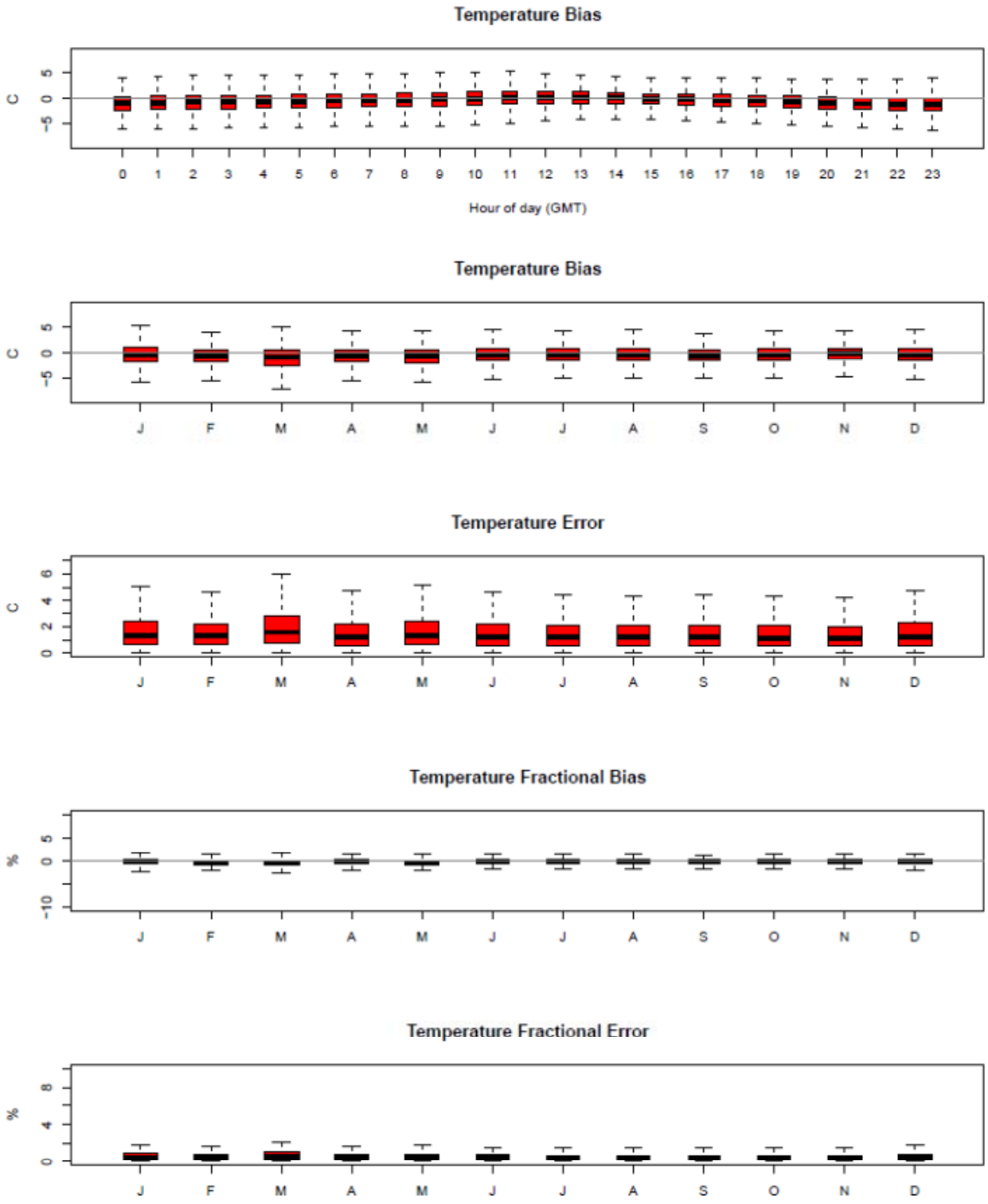

Figure 3.3.3. Distribution of hourly temperature bias by hour and hourly temperature bias, error, fractional bias, and fractional error by month for the 4NE domain.

3.3.3 Mixing Ratio

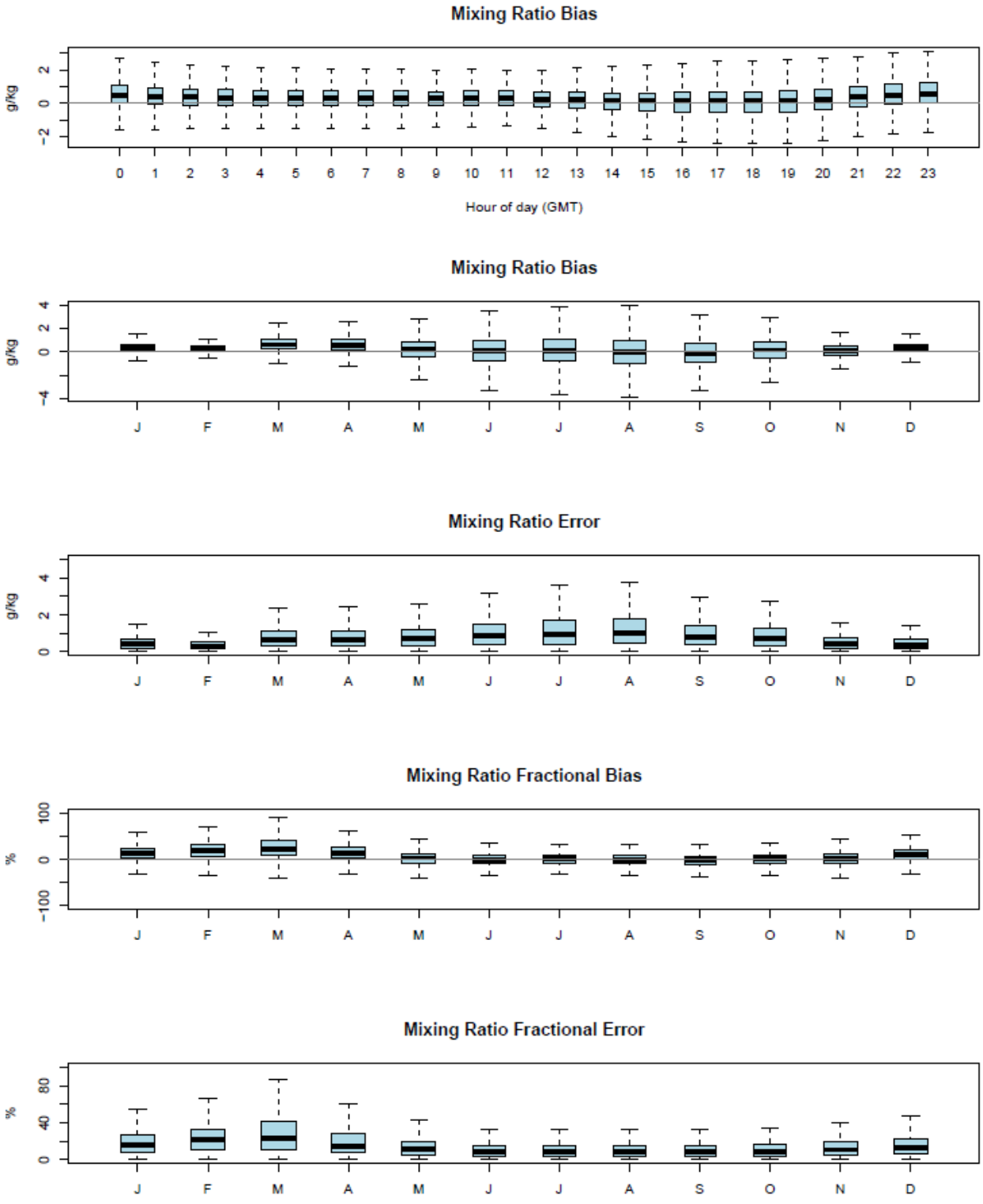

Figure 3.3.4. Distribution of hourly mixing ratio bias by hour and hourly mixing ratio bias, error, fractional bias, and fractional error by month for the 4NE domain.

3.3.4 Precipitation

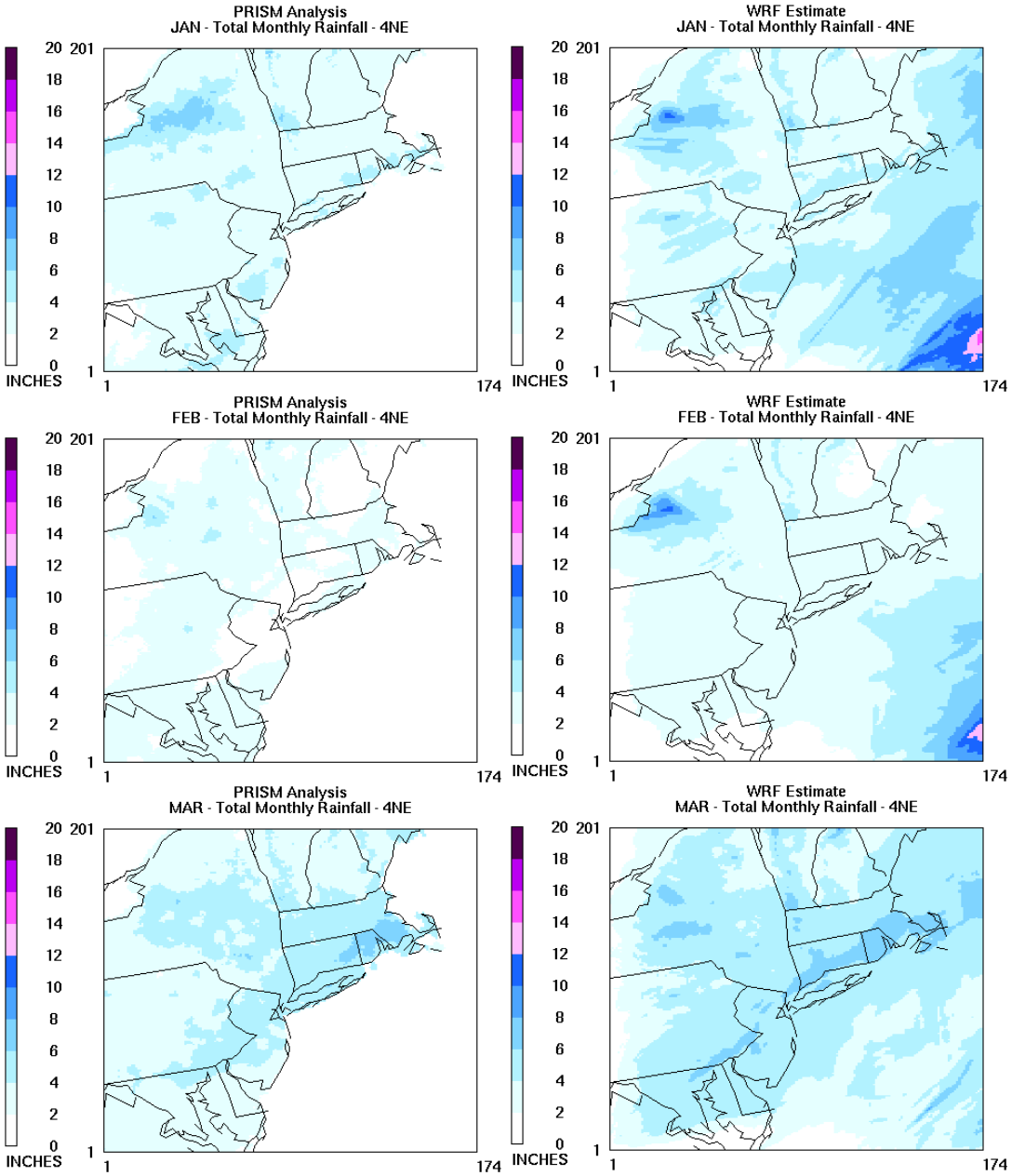

Figure 3.3.5. PRISM analysis (left) and WRF (right) estimated monthly total rainfall for January, February and March for the 4NE domain.

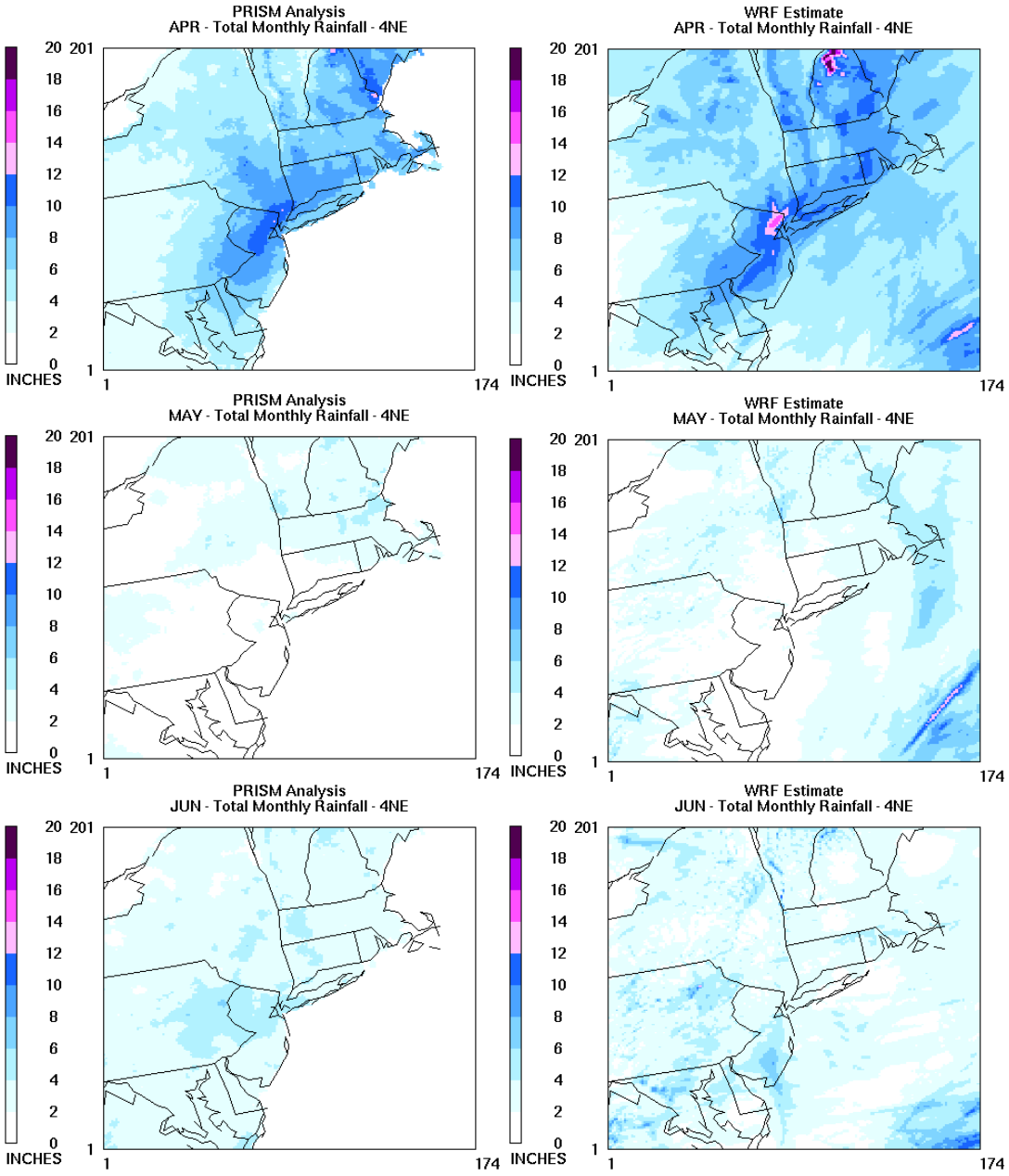

Figure 3.3.6. PRISM analysis (left) and WRF (right) estimated monthly total rainfall for April, May and June for the 4NE domain.

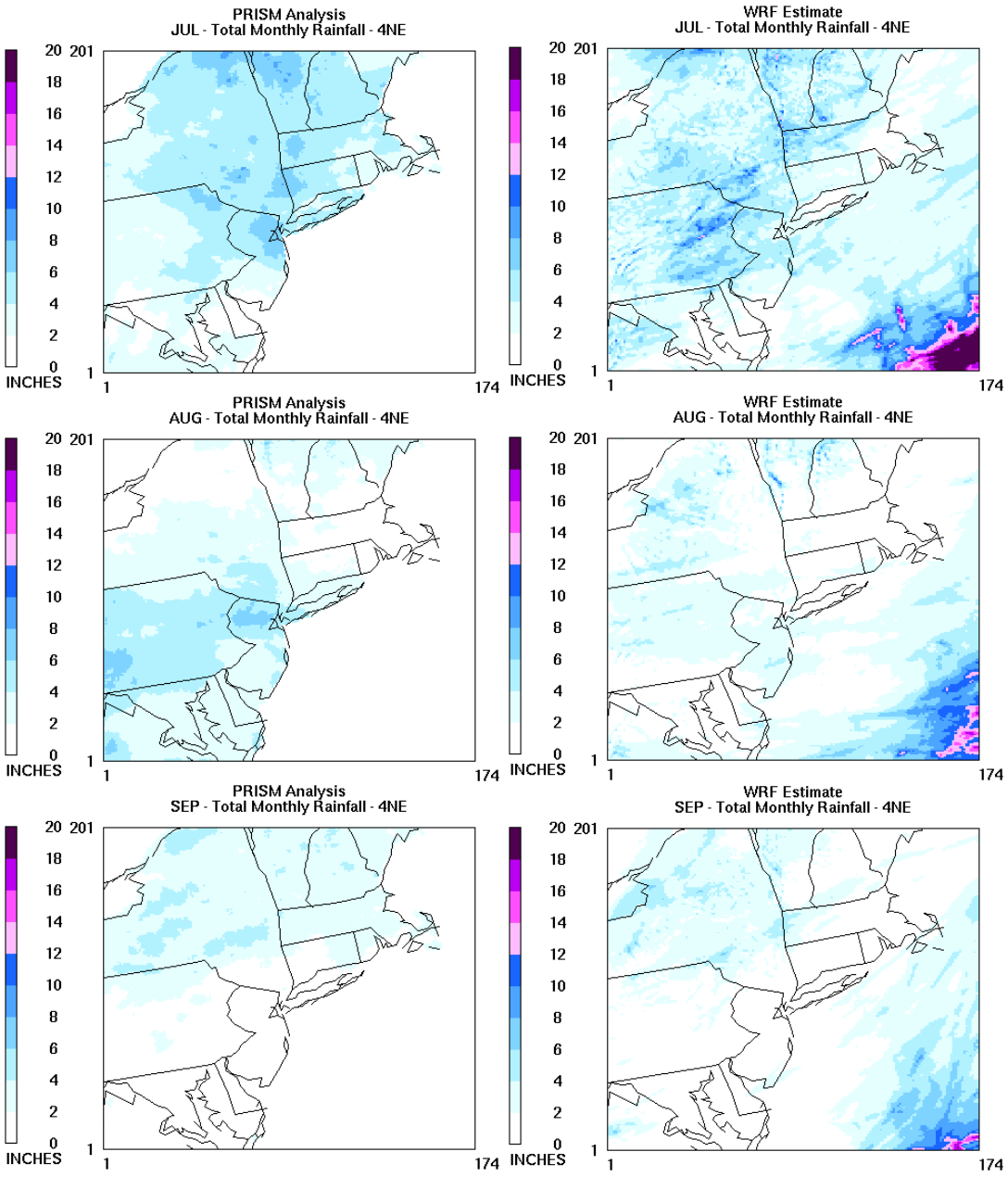

Figure 3.3.7. PRISM analysis (left) and WRF (right) estimated monthly total rainfall for July, August and September for the 4NE domain.

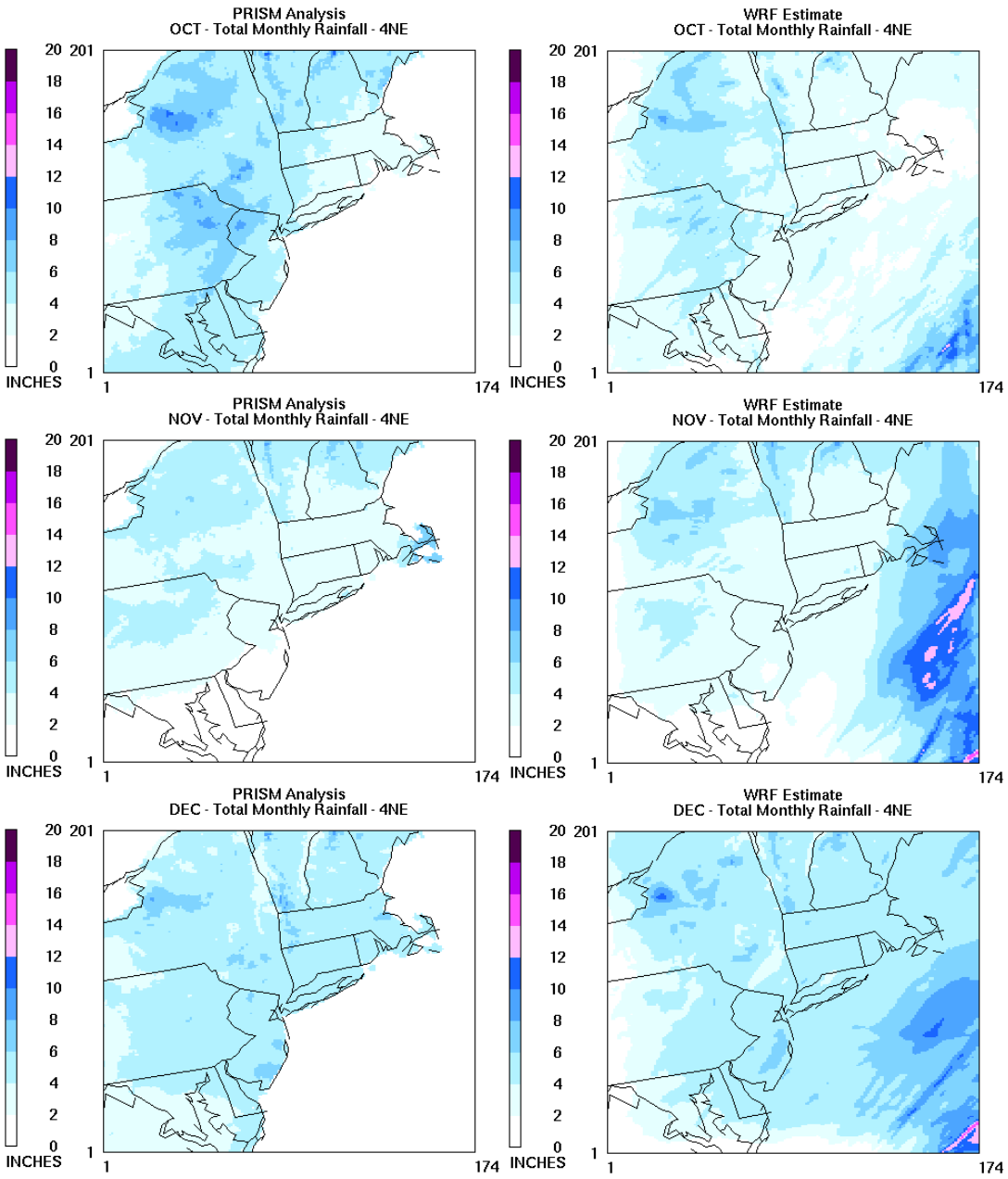

Figure 3.3.8. PRISM analysis (left) and WRF (right) estimated monthly total rainfall for January, February and March for the 4NE domain.

3.3.5 Maximum Predicted PBL

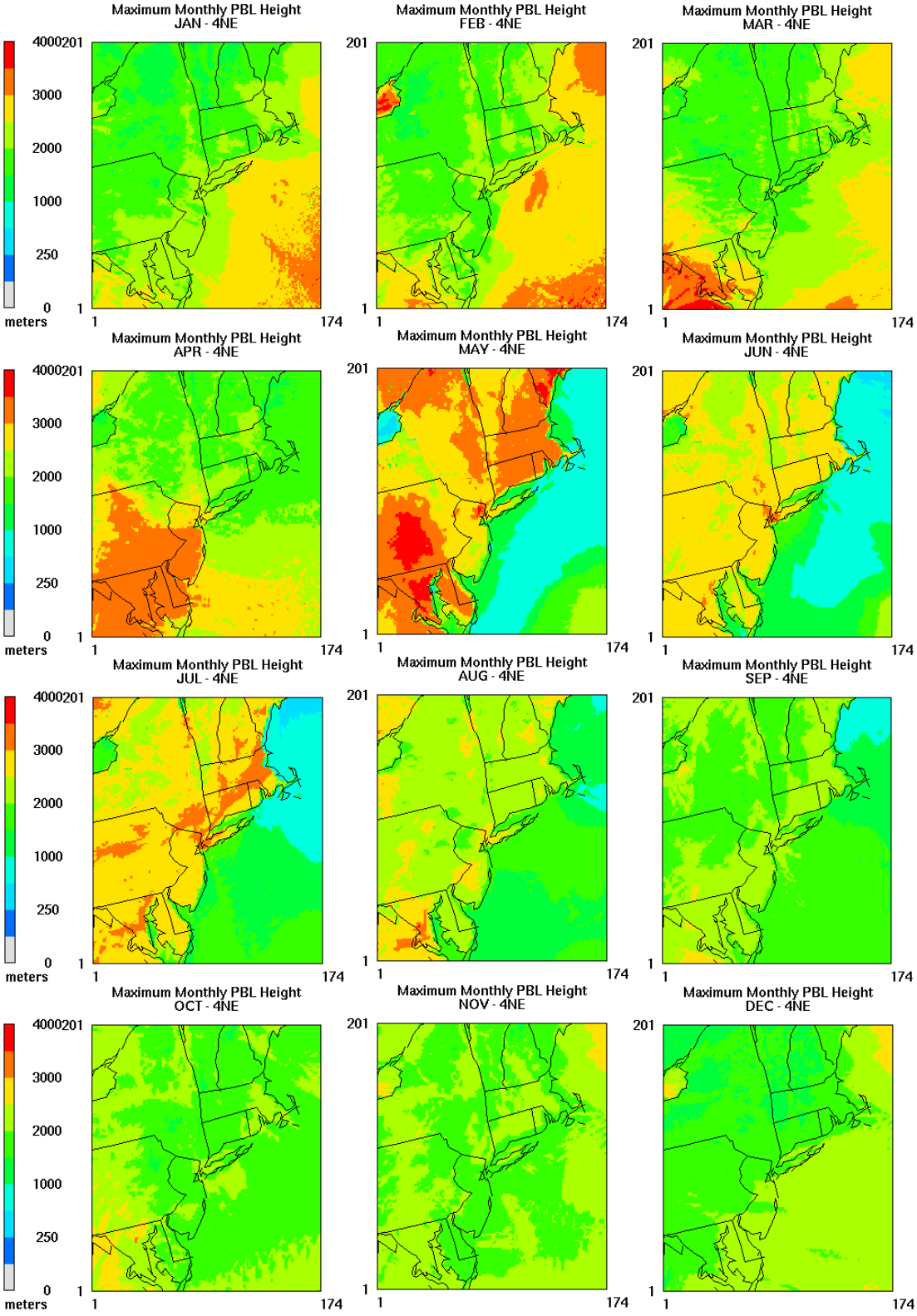

Figure 3.3.9. Monthly maximum PBL heights estimated by WRF for the 4NE domain.

3.3.6 Solar Radiation

Photosynthetically activated radiation (PAR) is a fraction of shortwave downward radiation and is an important input for the biogenic emissions model for estimating isoprene (Carlton and Baker, 2011). Isoprene emissions are important for regional ozone chemistry and play a role in secondary organic aerosol formation. Radiation performance evaluation also gives an indirect assessment of how well the model captures cloud formation during daylight hours.

Shortwave downward radiation estimates are compared to surface based measurements made at SURFRAD and ISIS network monitors for the 4NE domain (Figure 3.3.10). Outliers are not plotted on these box plots to emphasize predominant features in model performance. The outer edges of the box represent the 25th and 75th percentiles and the edges of the whiskers represent the 10th and 90th percentiles of the distributions. These plots show the entire distribution of hourly bias (model-observation) by month and by hour of the day.

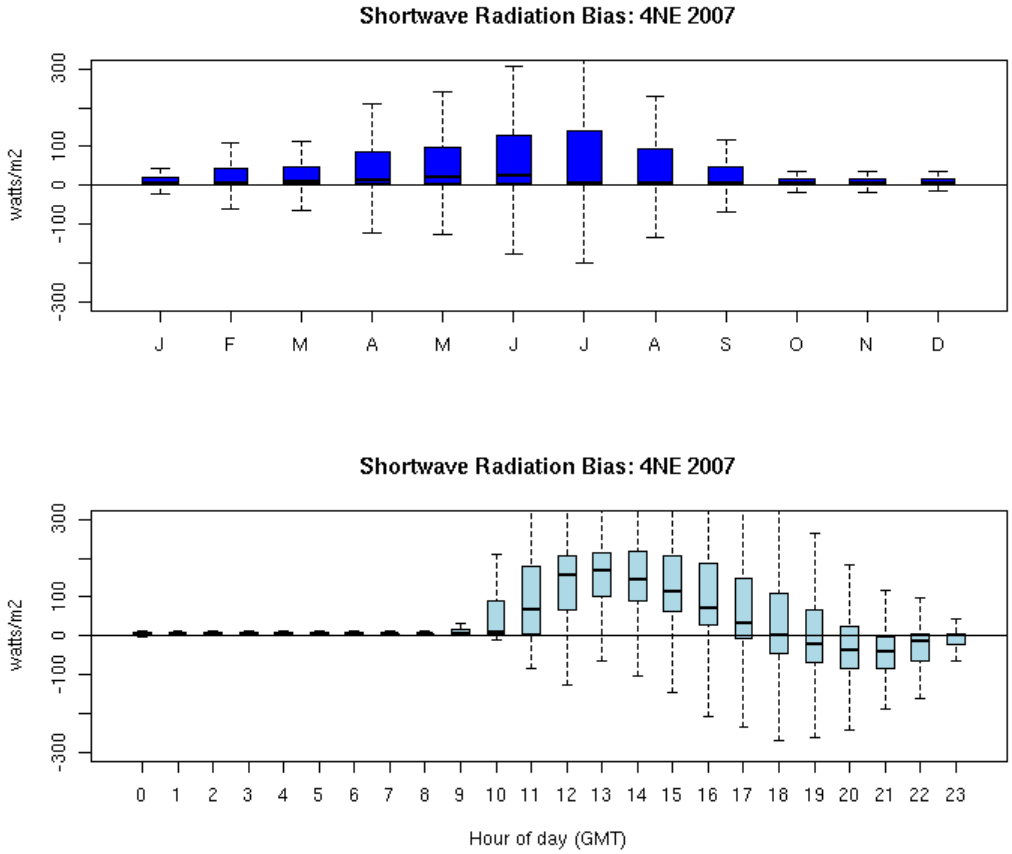

Figure 3.3.10 Distribution of hourly shortwave radiation bias by month (top) and by hour of the day (bottom) for the 4NE domain.

3.4 California (4CALNEX) Performance

3.4.1 Wind Field

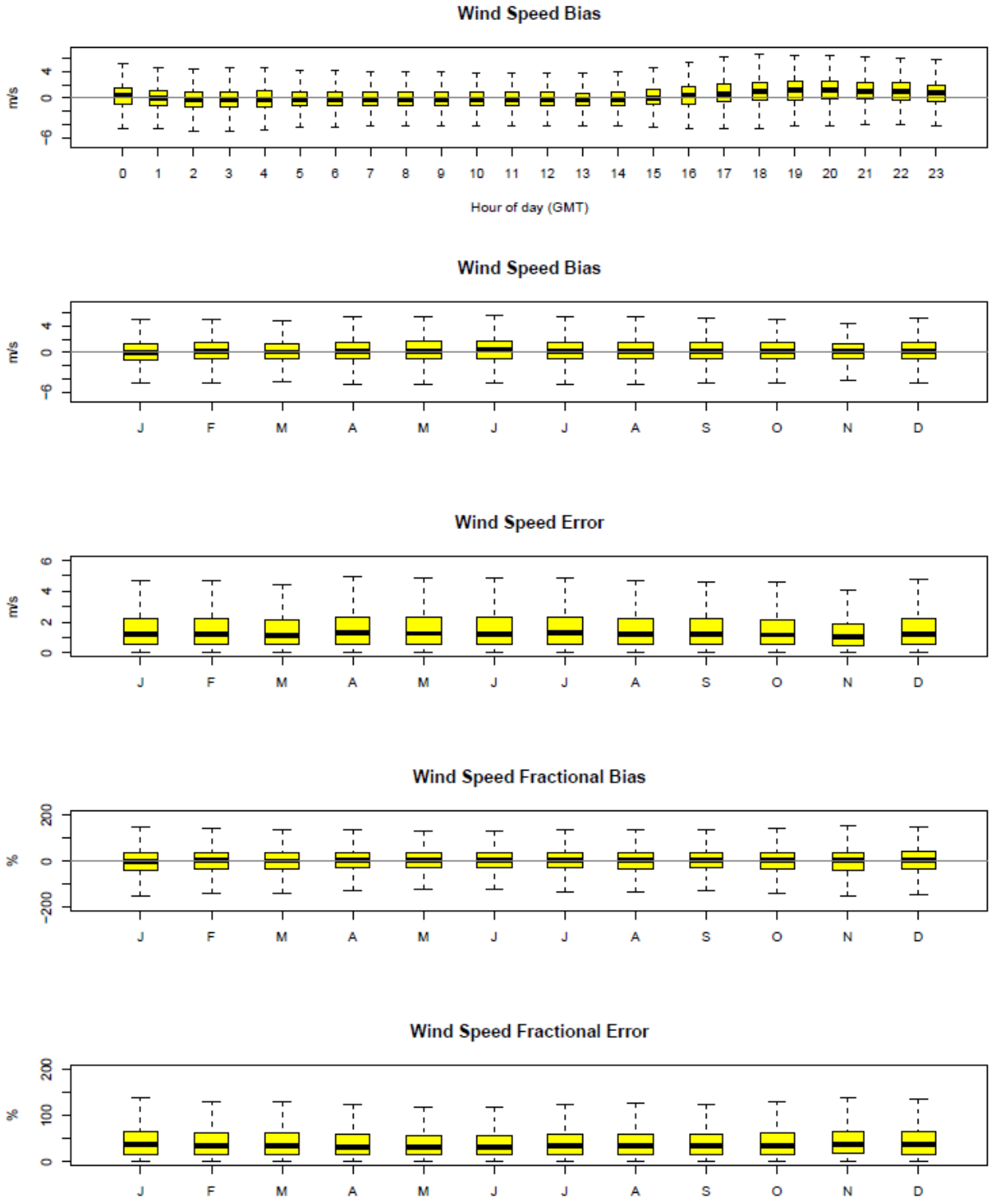

Figure 3.4.1. Distribution of hourly wind speed bias by hour and hourly wind speed bias, error, fractional bias, and fractional error by month for 4CALNEX domain.

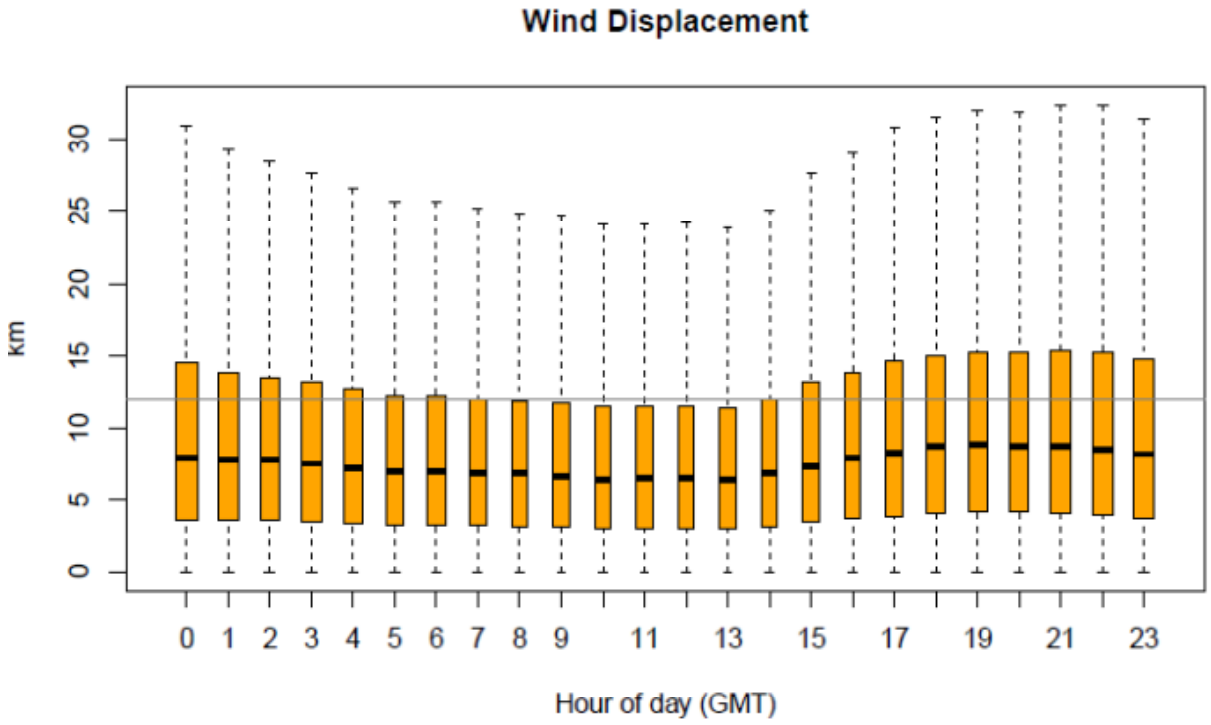

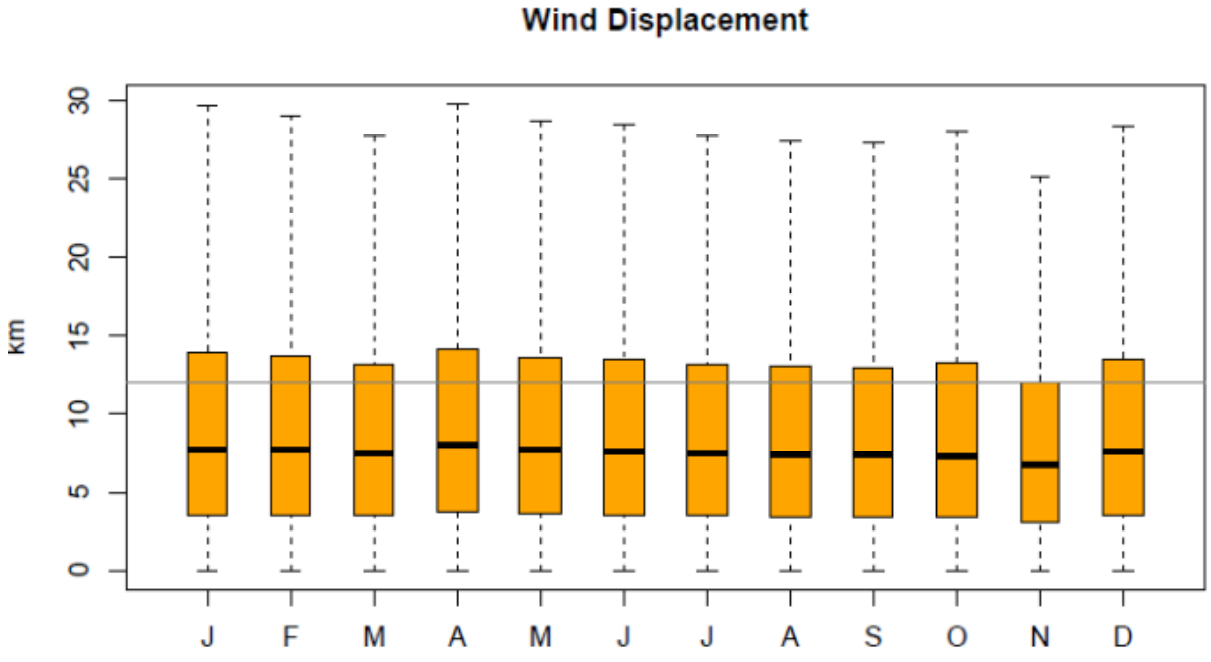

Figure 3.4.2. Distribution of hourly wind displacement by hour and month for the 4CALNEX domain.

3.4.2 Temperature

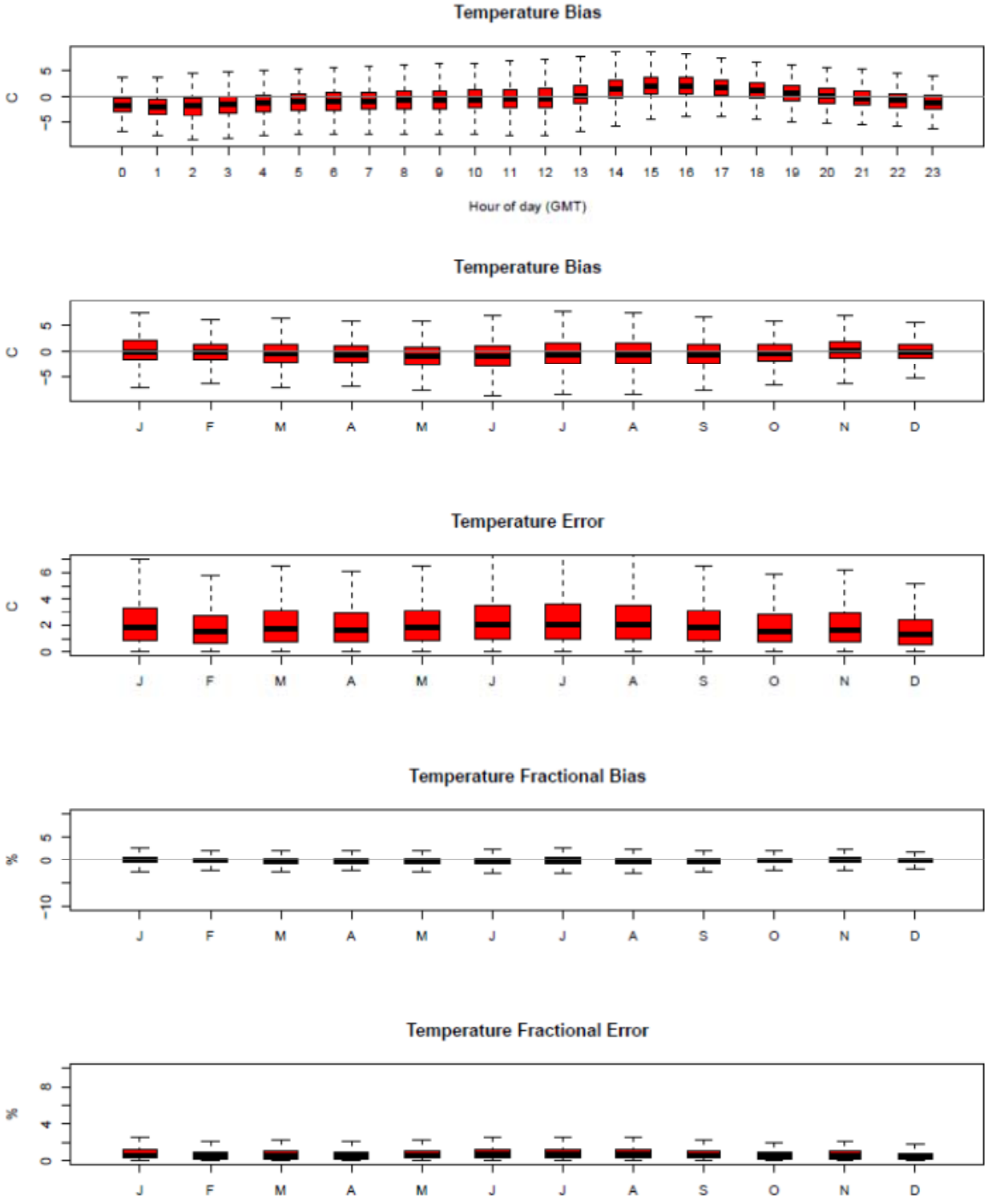

Figure 3.4.3. Distribution of hourly temperature bias by hour and hourly temperature bias, error, fractional bias, and fractional error by month for the 4CALNEX domain.

3.4.3 Mixing Ratio

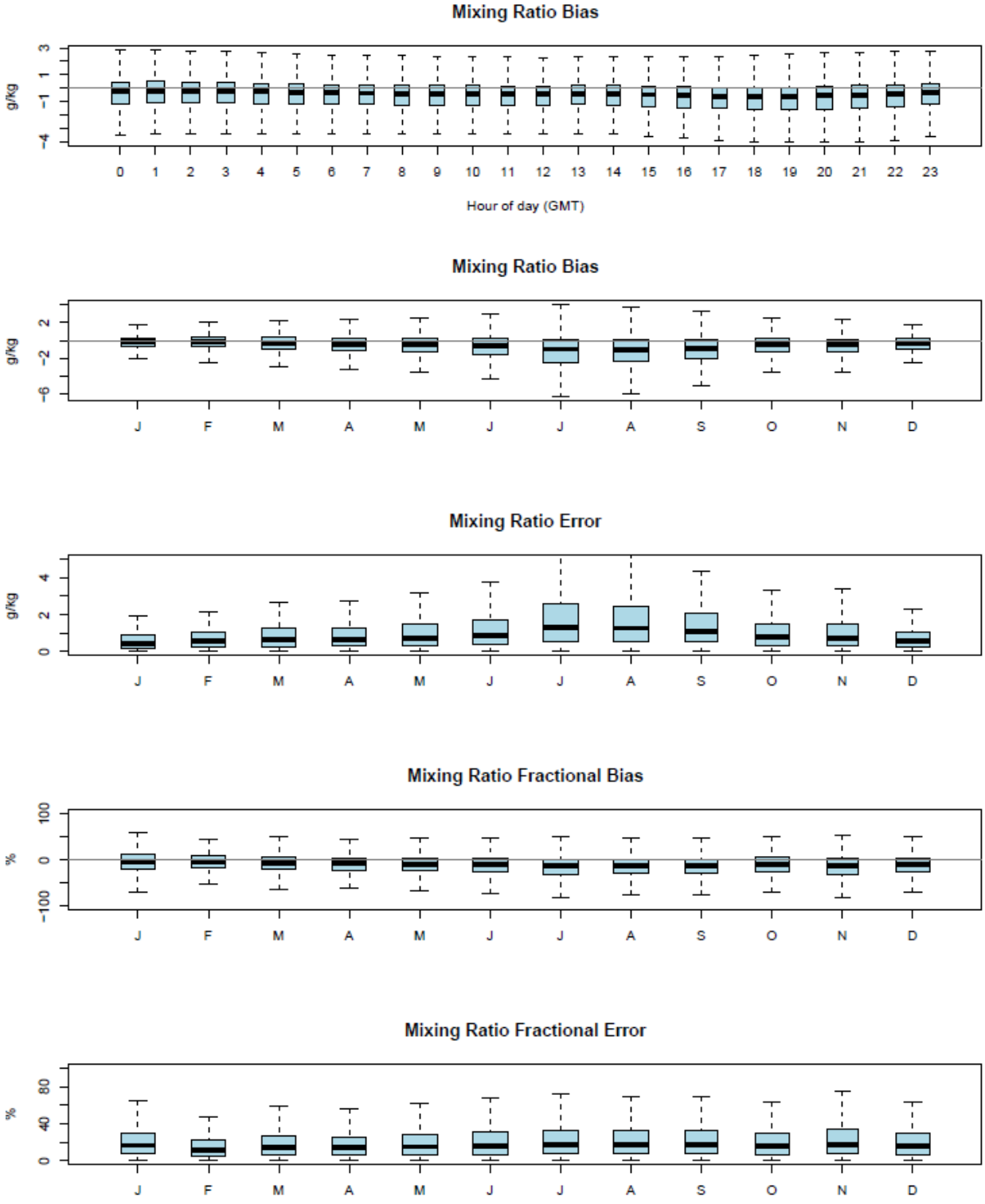

Figure 3.4.4. Distribution of hourly mixing ratio bias by hour and hourly mixing ratio bias, error, fractional bias, and fractional error by month for the 4CALNEX domain.

3.4.4 Precipitation

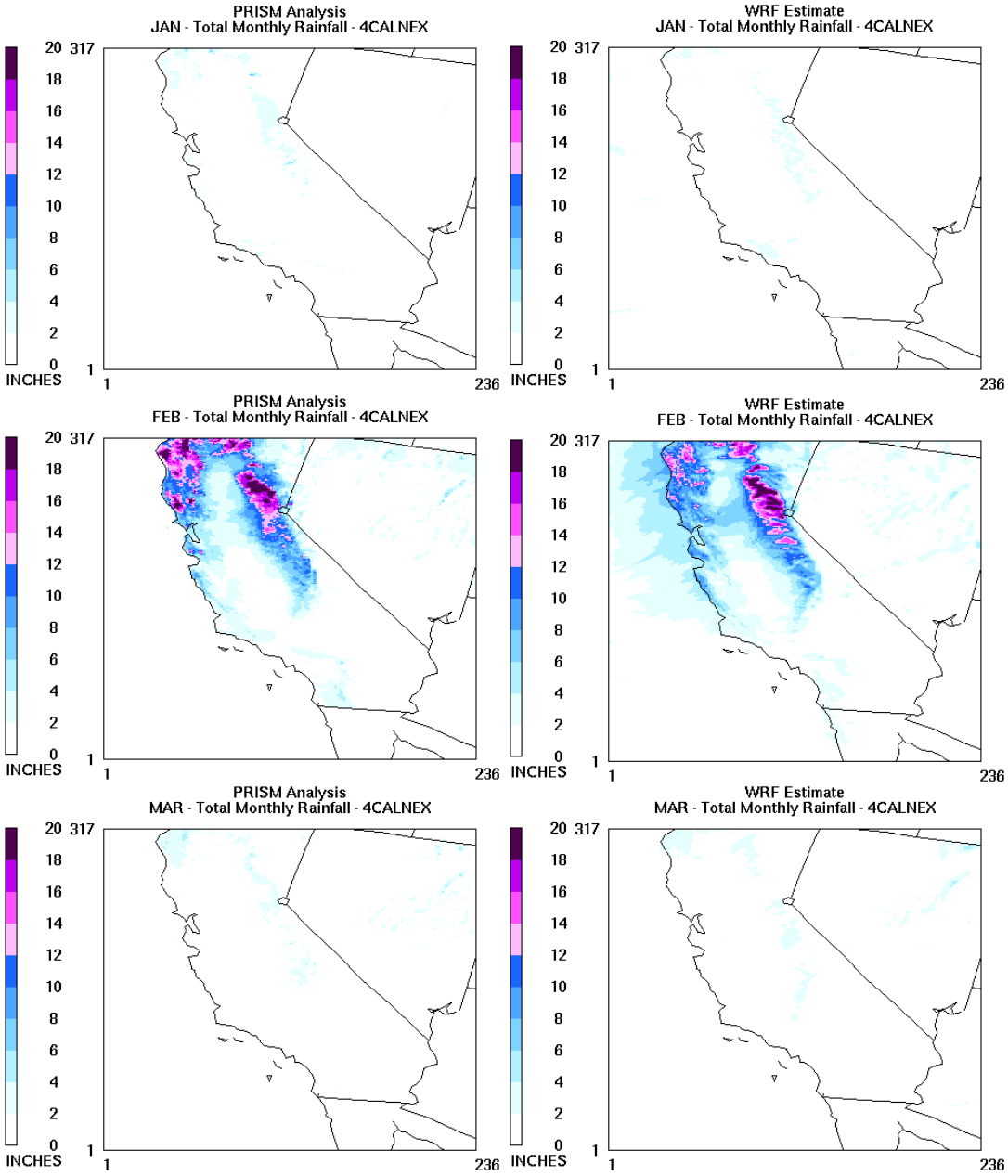

Figure 3.4.5. PRISM analysis (left) and WRF (right) estimated monthly total rainfall for January, February and March for the 4CALNEX domain.

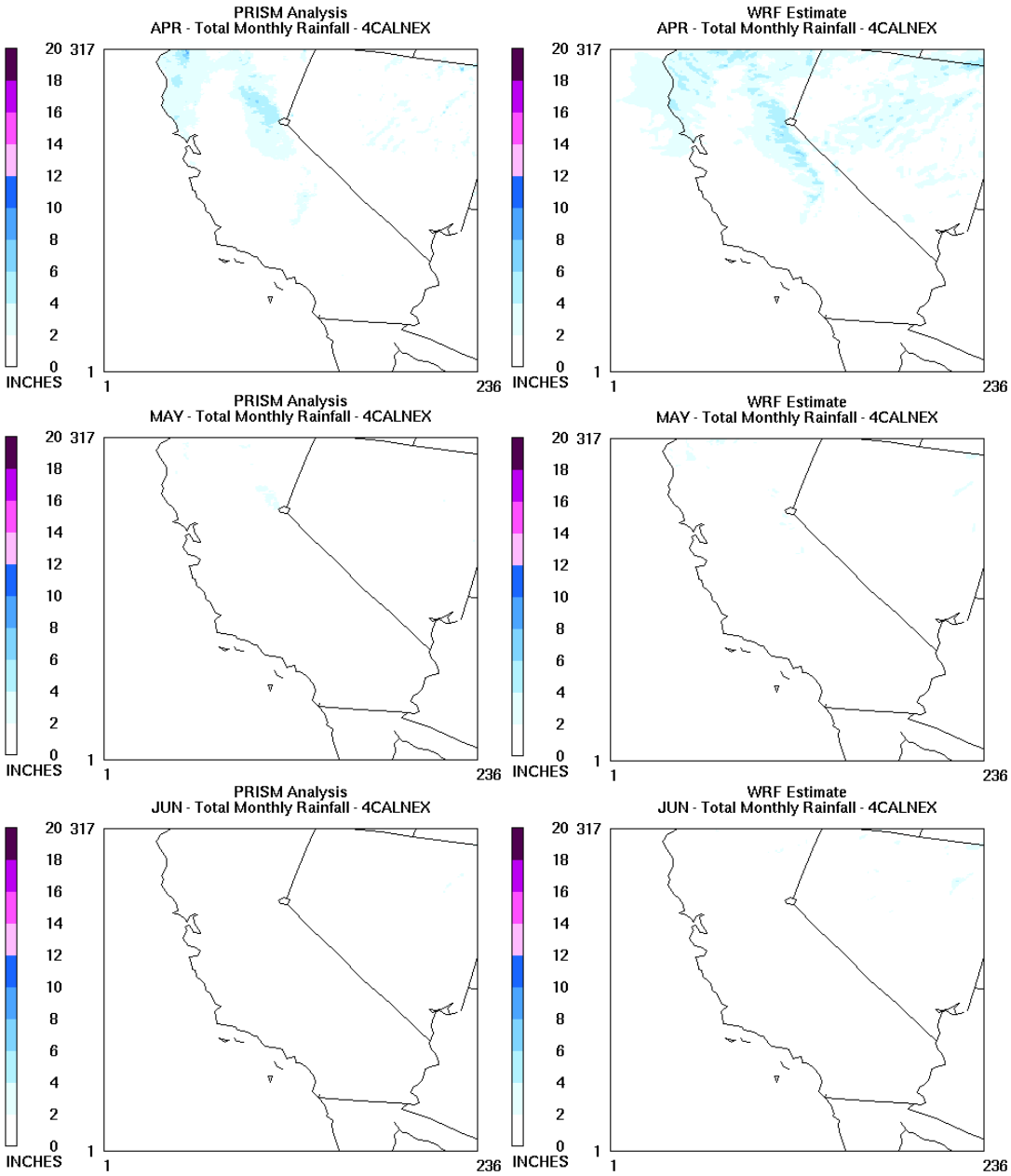

Figure 3.4.6. PRISM analysis (left) and WRF (right) estimated monthly total rainfall for April, May and June for the 4CALNEX domain.

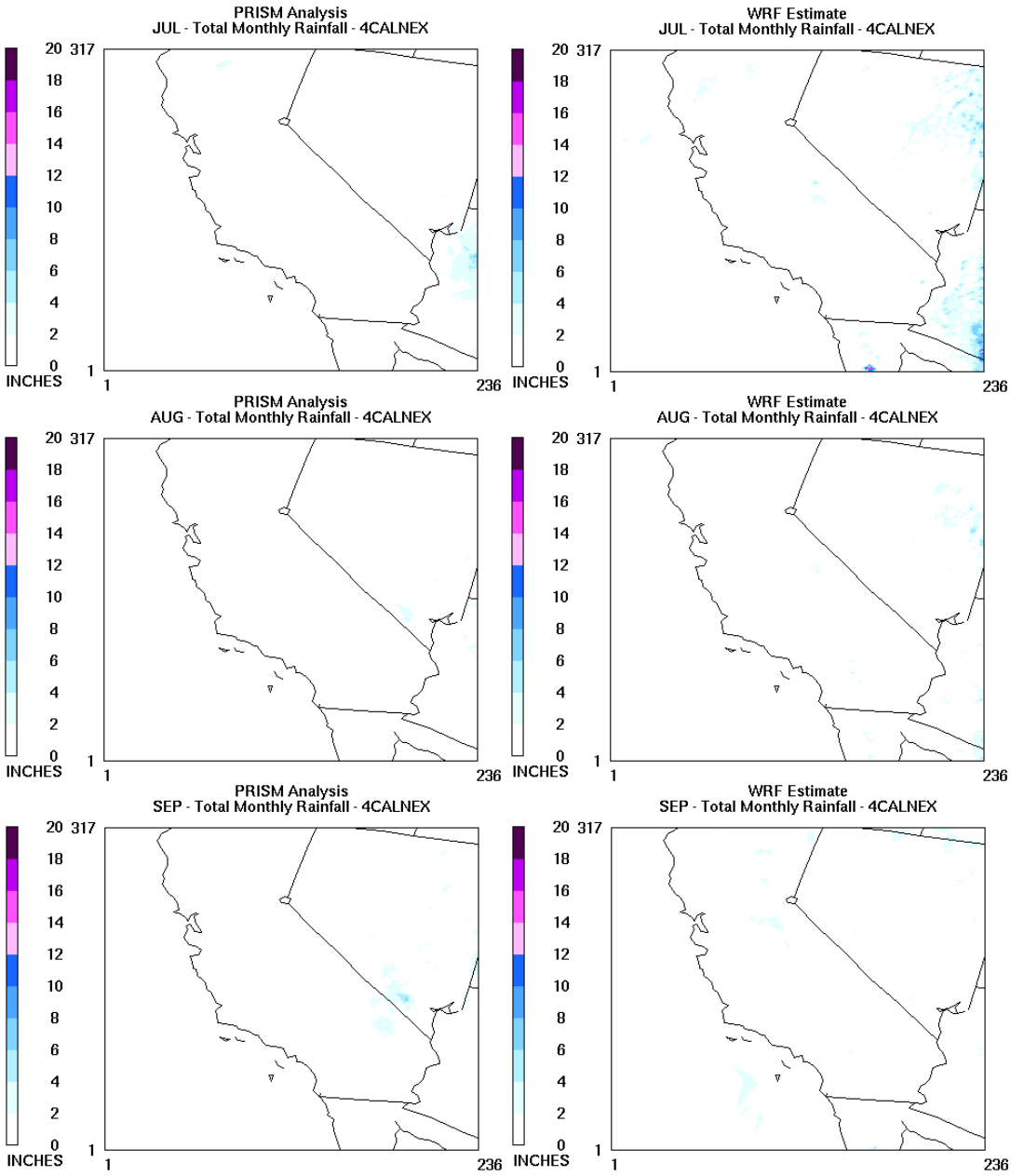

Figure 3.4.7. PRISM analysis (left) and WRF (right) estimated monthly total rainfall for July, August and September for the 4CALNEX domain.

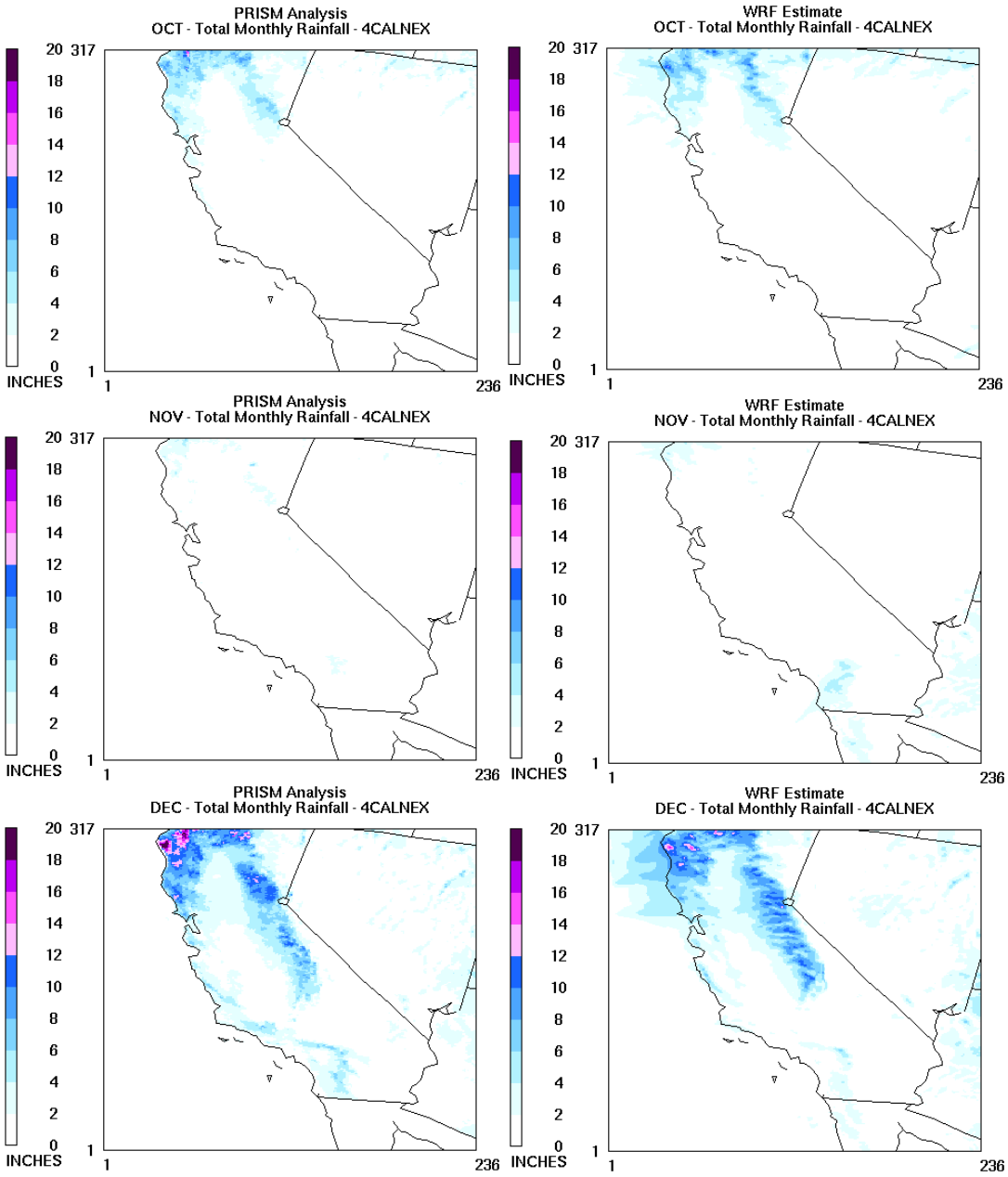

Figure 3.4.8. PRISM analysis (left) and WRF (right) estimated monthly total rainfall for October, November and December for the 4CALNEX domain.

3.4.5 Maximum Predicted PBL

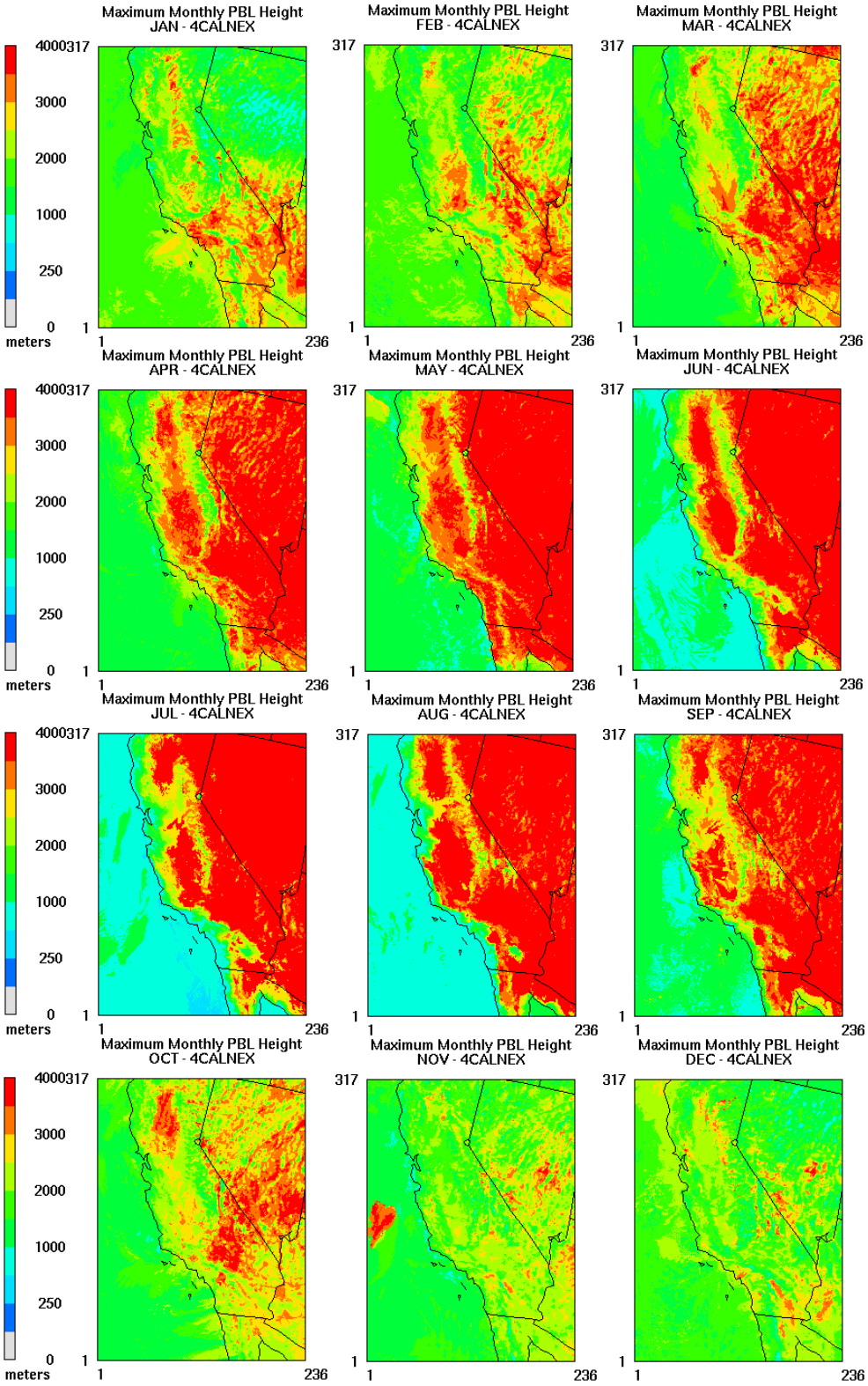

Figure 3.4.9. Monthly maximum PBL heights estimated by WRF for the 4CALNEX domain.

3.4.6 Solar Radiation

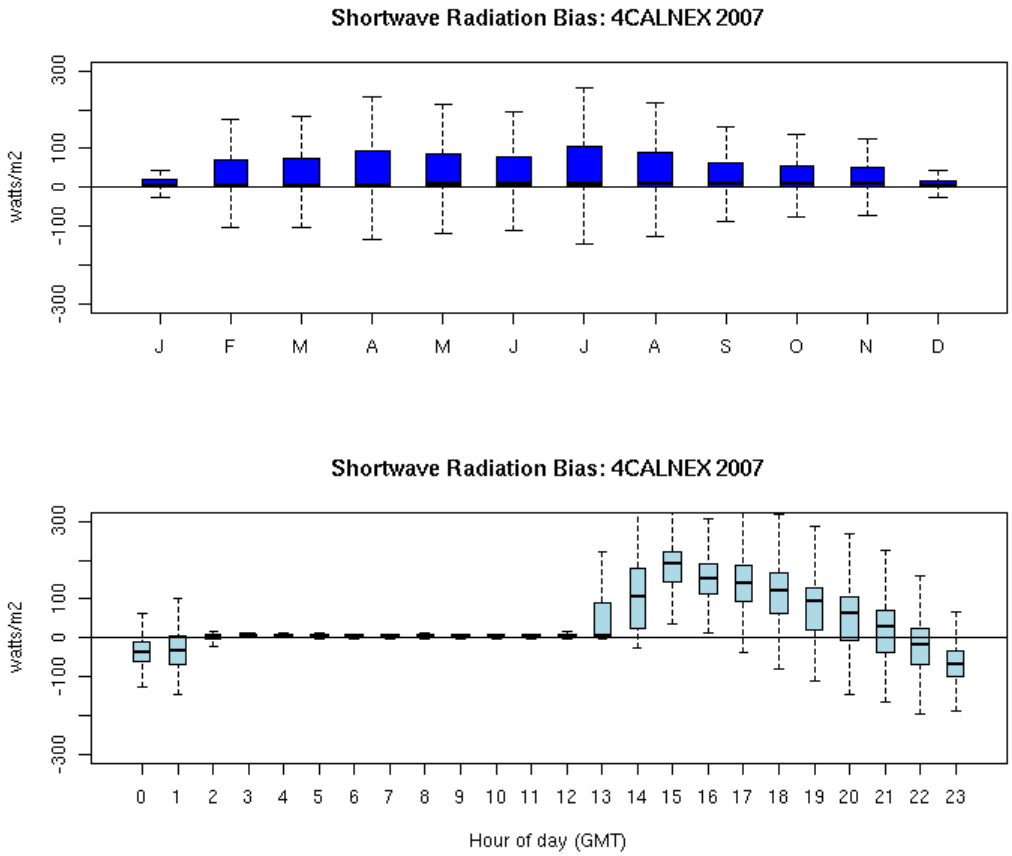

Figure 3.4.10 Distribution of hourly shortwave radiation bias by month (top) and by hour of the day (bottom) for the 4CALNEX domain.

4 REFERENCES

Boylan, J.W., Russell, A.G., 2006. PM and light extinction model performance metrics, goals, and criteria for three-dimensional air quality models. Atmospheric Environment 40, 4946-4959.

Carlton, A.G., Baker, K.R., 2011. Photochemical Modeling of the Ozark Isoprene Volcano: MEGAN, BEIS, and Their Impacts on Air Quality Predictions. Environmental Science & Technology 45, 4438-4445.

Chou, M.-D. and Suarez, M.J., 1994. An efficient thermal infrared radiation parameterization for use in general circulation model. NASA Technical Memo 104606, Vol. 3, 85pp.

Cooper, O.R., Stohl, A., Hubler, G., Hsie, E.Y., Parrish, D.D., Tuck, A.F., Kiladis, G.N., Oltmans, S.J., Johnson, B.J., Shapiro, M., Moody, J.L., Lefohn, A.S., 2005. Direct Transport of Midlatitude Stratospheric Ozone into the Lower Troposphere and Marine Boundary Layer of the

Pacific Ocean. Journal of Geophysical Research – Atmospheres 110, D23310, doi:10.1029/2005JD005783.

Ek, M.B., Mitchell, K.E., Lin, Y., Grunmann, P., Rogers, E., Gayno, G., Koren, V., and Tarpley, J.D., 2003. Implementation of the upgraded Noah land-surface model in the NCEP operational mesoscale Eta model. Journal of Geophysical Research 108(D22), 8851, doi:10.1029/2002JD003296

ENVIRON, 2008. User's Guide Comprehensive Air Quality Model with Extensions. ENVIRON International Corporation, Novato.

Fast, J. D., Gustafson Jr., W. I., Berg, L.K., Shaw, W.J., Pekour, M., Shrivastava, M., Barnard, J.C., Ferrare, R.A., Hostetler, C.A., Hair, J.A., Erickson, M., Jobson, B.T., Flowers, B., Dubey, M.K., Springston, S., Pierce, R.B., Dolislager, L., Pederson, J., and Zaveri, R.A., 2012. Transport and mixing patterns over Central California during the carbonaceous aerosol and radiative effects study (CARES), Atmospheric Chemistry and Physics, 12, 1759-1783.

Gilliam, R.C., Pleim, J.E., 2010. Performance Assessment of New Land Surface and Planetary Boundary Layer Physics in the WRF-ARW. Journal of Applied Meteorology and Climatology 49, 760-774.

Iacono, M.J., Delamere, J.S., Mlawer, E.J., Shephard, M.W., Clough, S.A., and Collins, W.D., 2008. Radiative forcing by long-lived greenhouse gases: calculations with the AER radiative transfer models, Journal of Geophysical Research 113, D13103, doi:10.1029/2008JD009944.

Janjic, Z. I., 1994. The Step-Mountain Eta Coordinate Model: Further Developments of the Convection, Viscous Sublayer, and Turbulence Closure Schemes. Monthly Weather Review 122, 927-945.

Kain, S., 2004. The Kain-Fritsch Convective Parameterization: An Update. Journal of Applied Meteorology and Climatology 43, 170-181.

Langford, A.O., Reid, S.J., 1998. Dissipation and Mixing of a Small-Scale Stratospheric Intrusion in the Upper Troposphere. Journal of Geophysical Research 103, 31265-31276.

Mlawer, E.J., Taubman, S.J., Brown, P.D., and Iacono, M.J., 1997. Radiative transfer for inhomogeneous atmospheres: RRTM, a validated correlated-k Model for the longwave. Journal of Geophysical Research 102, 16663-16682.

Otte, T.L., Pleim, J.E., 2010. The Meteorology-Chemistry Interface Processor (MCIP) for the CMAQ modeling system: updates through MCIPv3.4.1. Geoscientific Model Development 3, 243-256.

Pleim, J.E., 2007. A combined local and non-local closure model for the atmospheric boundary layer. Part 1: Model description and testing. Journal of Applied Meteorology and Climatology 46, 1383-1395.

Pleim, J.E., and Xiu, A., 2003. Development of a land surface model. Part II: Data assimilation. Journal of Applied Meteorology 42, 1811-1822.

Skamarock, W.C., Klemp, J.B., Dudhia, J., Gill, D.O., Barker, D.M., Duda, M.G., Huang, X., Wang, W., Powers, J.G., 2008. A Description of the Advanced Research WRF Version 3.

Thompson, G., Field, P.R., Rasmussen, R.M., Hall, W.D., 2008. Explicit forecasts of winter precipitation using an improved bulk microphysics scheme. Part II: Implementation of a New Snow Parameterization. Monthly Weather Review 136, 5095-5115.

APPENDIX A

Climatic Charts for 2007

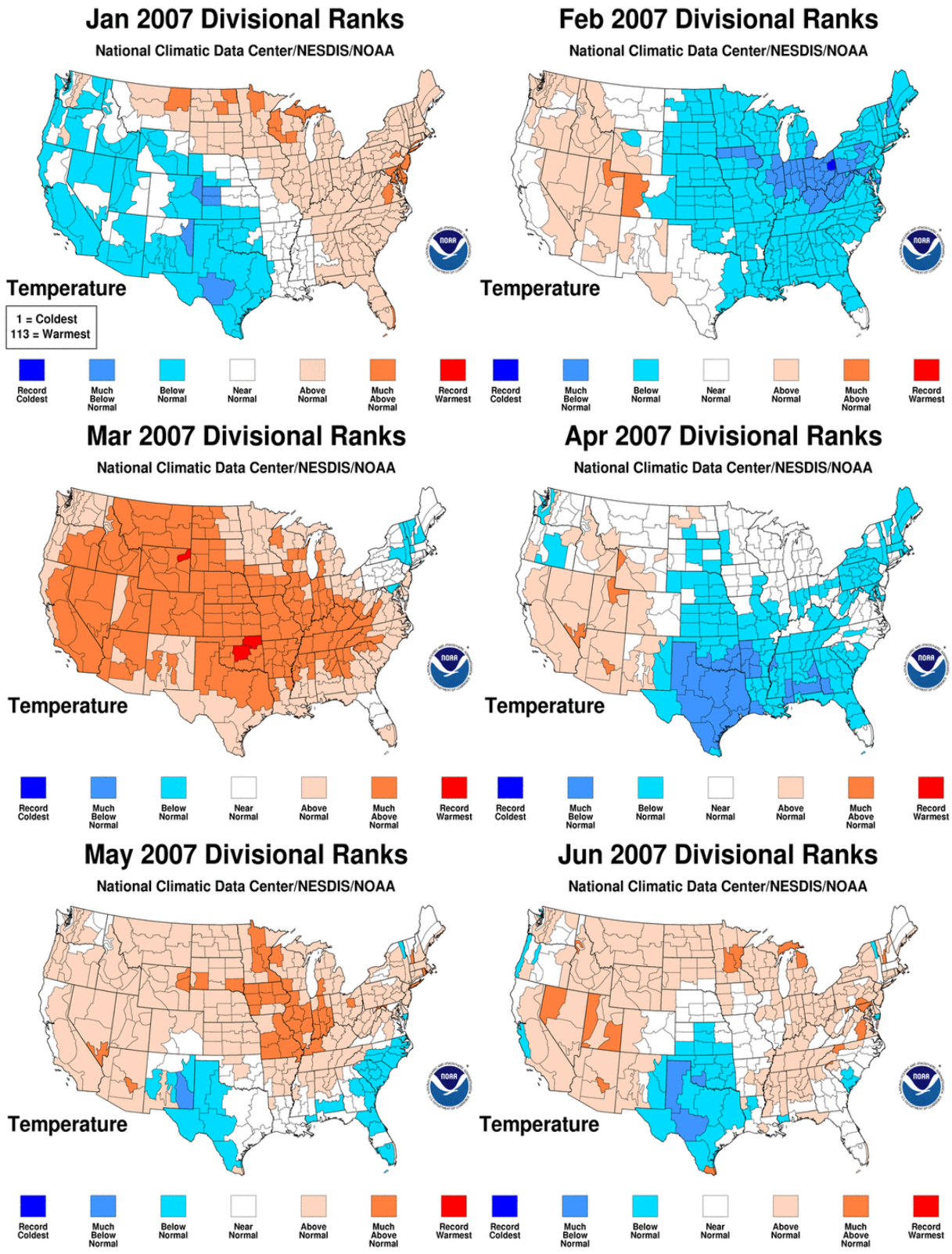

Figure A.1 Climatic temperature rankings by climate division: January to June 2007. http://www.ncdc.noaa.gov/temp-and-precip/maps.php

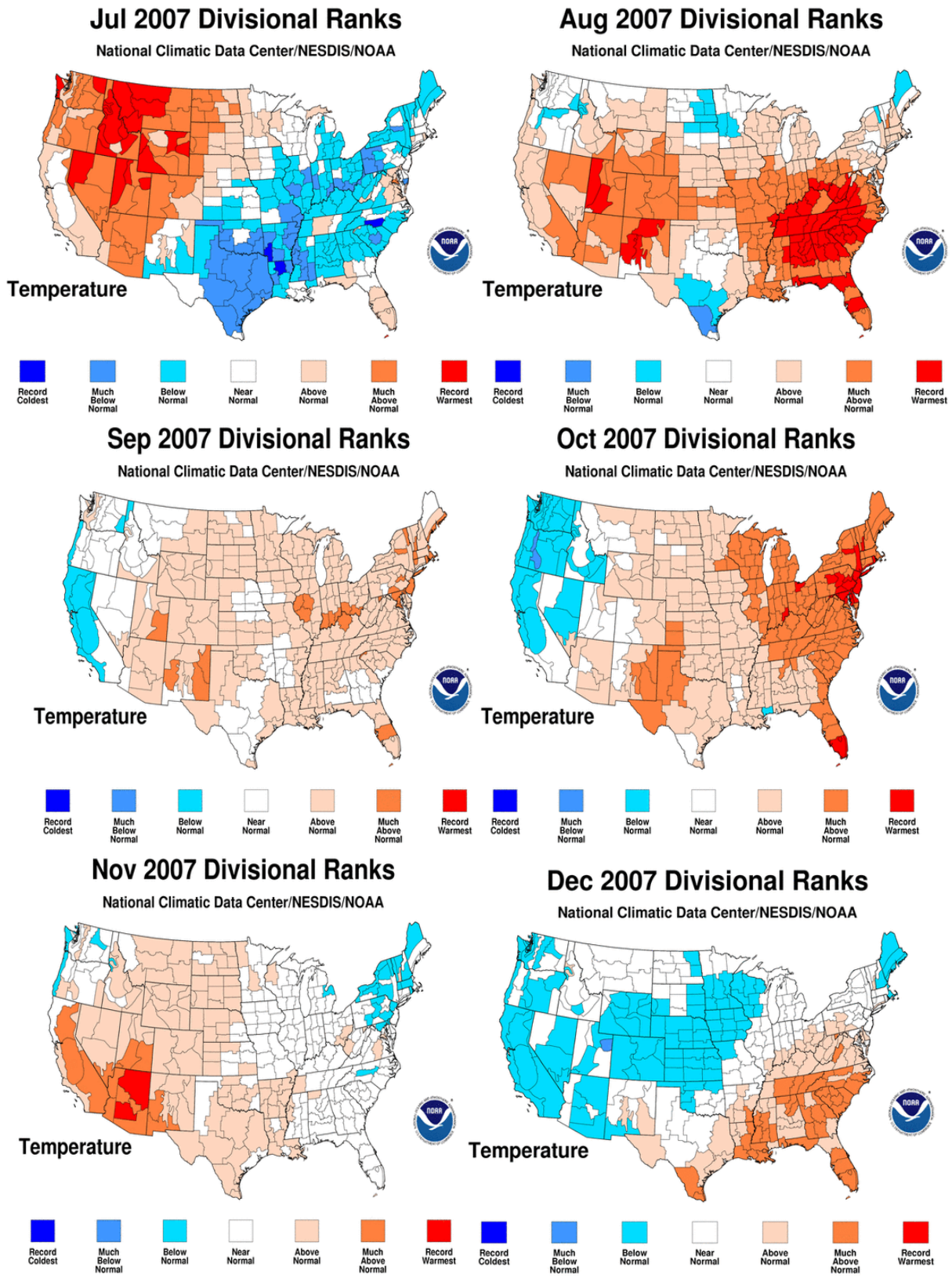

Figure A.2 Climatic temperature rankings by climate division: July to December 2007. http://www.ncdc.noaa.gov/temp-and-precip/maps.php

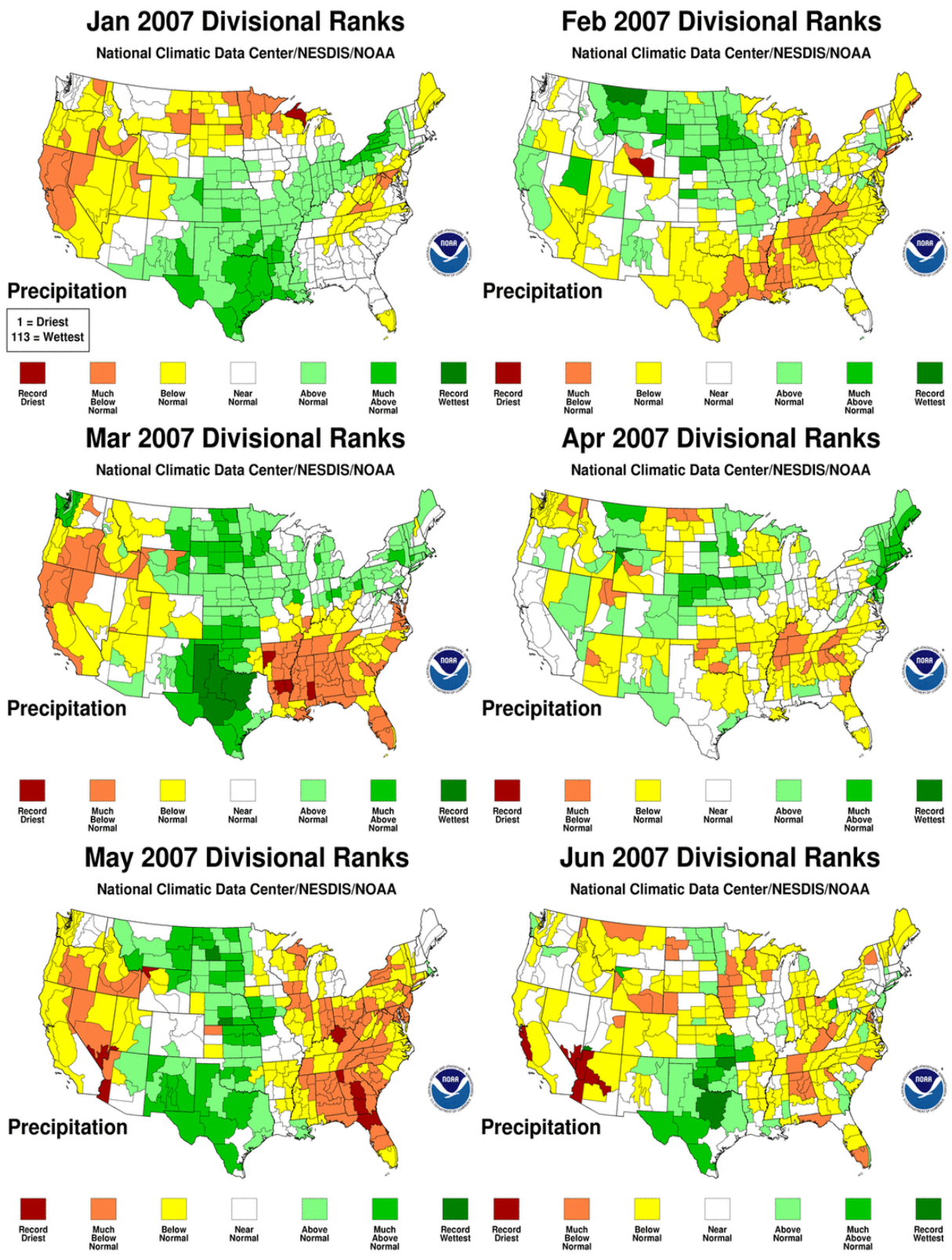

Figure A.3 Climatic rainfall rankings by climate division: January to June 2007. http://www.ncdc.noaa.gov/temp-and-precip/maps.php

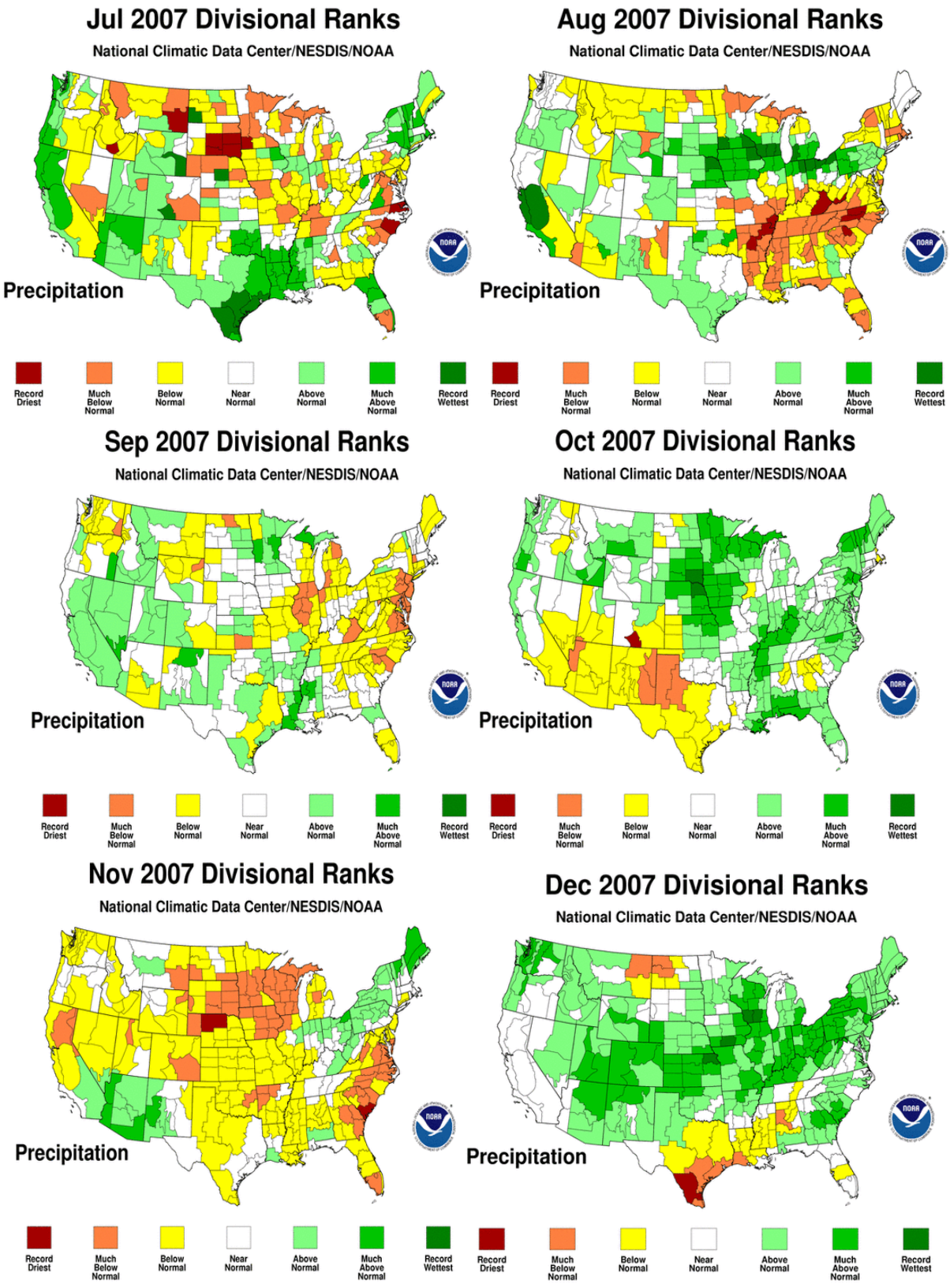

Figure A.4 Climatic rainfall rankings by climate division: July to December 2007. http://www.ncdc.noaa.gov/temp-and-precip/maps.php